HYPERABRUPT VARACTOR VOLTAGE-CONTROLLED OSCILLATORS

D. D. Mawhinney and J. J. Napoleon
RCA LABORATORIES
Princeton, New Jersey 08540

OCTOBER 1977

FINAL REPORT
For the period 30 June 1975 to 30 November 1976

Contract No. N00039-75-C-0474

UNCLASSIFIED

SECURITY CLASSIFICATION OF THIS PAGE (When Data Entered)

REPORT DOCUMENTATION PAGE		READ INSTRUCTIONS BEFORE COMPLETING FORM
1. REPORT NUMBER	2. GOVT ACCESSION NO.	3. RECIPIENT'S CATALOG NUMBER
4. TITLE (and Subtitle) (6) HYPERABRUPT VARACTOR VOLTAGE-CONTROLLED OSCILLATORS		5. TYPE OF REPORT & PERIOD COVERED (9) Final Report, 30 Jun 75 - 30 Nov 76 (6-30-75 to 11-30-76)
		6. PERFORMING ORG. REPORT NUMBER (14) PRRL-77-R-45
7. AUTHOR(s) (10) D. D. Mawhinney [redacted] J. J. Napoleon		8. CONTRACT OR GRANT NUMBER(s) (15) N0039-75-C-0474
9. PERFORMING ORGANIZATION NAME AND ADDRESS RCA Laboratories Princeton, New Jersey 08540		10. PROGRAM ELEMENT, PROJECT, TASK AREA & WORK UNIT NUMBERS
11. CONTROLLING OFFICE NAME AND ADDRESS Naval Electronic Systems Command Washington, D.C. 20360		12. REPORT DATE (11) Oct[redacted]977 13. NUMBER OF PAGES 79 (12) 79p.
14. MONITORING AGENCY NAME & ADDRESS (if different from Controlling Office)		15. SECURITY CLASS. (of this report) Unclassified 15a. DECLASSIFICATION/DOWNGRADING SCHEDULE N/A

16. DISTRIBUTION STATEMENT (of this Report)

DISTRIBUTION STATEMENT A
Approved for public release;
Distribution Unlimited

DDC RECEIVED DEC 12 1977

17. DISTRIBUTION STATEMENT (of the abstract entered in Block 20, if different from Report)

299 000

18. SUPPLEMENTARY NOTES

19. KEY WORDS (Continue on reverse side if necessary and identify by block number)

Varactor
Hyperabrupt Varactor
Gallium Arsenide Varactor
Voltage-Controlled Oscillator (VCO)
Set-on VCO

20. ABSTRACT (Continue on reverse side if necessary and identify by block number)

A method for fabricating and processing plated heat sink hyperabrupt gallium arsenide varactors for use in microwave voltage-controlled oscillators was developed and evaluated during this program. VCOs fabricated with these varactors demonstrated considerably improved linearity and reduced tuning voltage requirements as compared with VCOs fabricated with conventional abrupt junction varactors.

DD FORM 1 JAN 73 1473

UNCLASSIFIED

SECURITY CLASSIFICATION OF THIS PAGE (When Data Entered)

20.

During the program, hyperabrupt gallium arsenide varactor wafers were grown in which values of γ from 0.5 to 2.0 were obtained and capacitance ratios as high as 30:1 were measured. In most cases, the carrier concentration profiles necessary to obtain the various hyperabrupt characteristics obtained were grown epitaxially by the hydride vapor synthesis technique using a programmed controller to introduce dopant at the required rates. The process was proven to have the capability to grow wafers which closely matched a desired profile. Because of the versatility of this controlled back-doping process, complicated structures can be grown such as the $p^{(+)}$-$n_{(0)}$-$n^{(+)}$-n-$p^{(+)}$ GaAs wafers which were used to produce electrolytically etched varactor diodes with integral heat sinks. These plated heat sink mounted varactors proved to have very low post tuning drift characteristics in VCOs compared with conventionally mounted GaAs varactors.

Voltage-controlled oscillators fabricated with the hypberabrupt GaAs varactors proved to have considerably better linearity and required lower tuning voltage swings than VCOs built using conventional step-abrupt junction varactors. Nearly straight line tuning characteristics were obtained over as much as 2 GHz in S-band, 2.5 GHz in X-band, and 4.5 GHz in Ku-band. Tuning voltage swings for these bandwidths were in the order of only 10 V rather than the 40 V which VCOs with conventional varactors would require. Less than expected overall bandwidth was obtained from these VCOs because of a significant reduction in the maximum junction capacitance of the hyperabrupt varactor in the presence of applied rf signal.

The basic design of a set-on VCO frequency memory was completed and demonstrated on a related program in X-band but was not implemented in Ku-band, as had been originally intended. In this related program, a VCO frequency memory system was designed, fabricated, and demonstrated which uses a combination of rapid open-loop set on, injection locking, and discriminator feedback control to respond to unknown frequency incoming pulses as short as 75 ns by setting a VCO to within 5 MHz of that frequency in less than 600 ns and holding it within the same accuracy for periods of time well beyond 80 μs. Longer duration input pulses produce exact set-on during the pulse through injection locking, but immediately following the input signal, there is a transient offset of approximately 400 ns while the feedback circuit stabilizes, after which the frequency error is reduced and held under 4 MHz for nearly 1 ms. Results obtained late in the hyperabrupt varactor VCO program have shown that comparable or better set-on VCO results should be obtainable using a single VCO covering 11 to 18 GHz.

PREFACE

This final report describes the work performed in the Microwave Technology Center of the RCA Laboratories, Princeton, New Jersey, from July, 1975 through November 1976 under Contract No. N00039-75-C-0474. Dr. F. Sterzer is the Laboratory Director and D. D. Mawhinney is the Project Engineer.

The author wishes to acknowledge the contributions of other RCA Laboratories' personnel who assisted with the work of this program. Foremost in this group is James J. Napoleon who recently passed away. It was his work in the development of varactor processing and measurement techniques which is reported herein and which made possible the considerable successful results which were obtained. His conscientious attention to detail and cooperative attitude as well as his personal friendliness will be sorely missed by his co-workers and friends.

The efforts of Herb Wolkstein in supplying valuable system and applications assistance as well as his contributions in program definition and liaison with NESC are gratefully acknowledged, as are the efforts of Paul Pelka and Henry Milgazo who fabricated and tested the numerous VCOs which were evaluated during this program. The specially profiled gallium arsenide hyperabrupt varactor material was grown and supplied by S. Jolly and J. Paczkowski under the direction of S. Y. Narayan who provided much overall guidance and assistance during the program.

The author also wishes to acknowledge the support and direction provided by Ron Wade and Nate Butler of Naval Electronic Systems Command on this program, and the assistance on the requirements and evaluation of the frequency memory system by Temple Timberlake of Naval Research Laboratory.

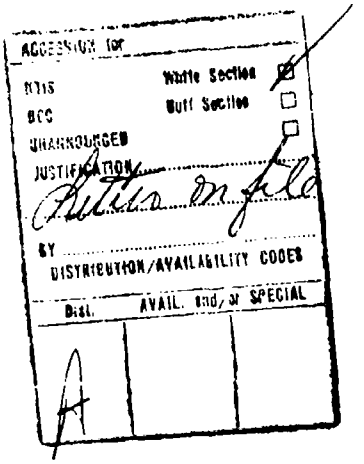

TABLE OF CONTENTS

LIST OF ILLUSTRATIONS

LIST OF ILLUSTRATIONS (Continued)

LIST OF ILLUSTRATIONS (Continued)

LIST OF TABLES

SECTION I

INTRODUCTION

The prime objective of this program was to develop improved *hyperabrupt gallium arsenide varactors* and to fabricate, demonstrate, and deliver an 11- to 18-GHz set-on voltage-controlled oscillators (VCO) breadboard assembly using these hyperabrupt gallium arsenide varactor diodes. The set-on VCO was to have stand-alone capability and the assembly was to contain threshold and logic circuits, an input signal limiter, and appropriate discriminators and linearizers. The design of the set-on VCO system was based on the work performed on a locked-open-loop VCO frequency memory system for NESC under Contract N00039-74-C-0227 and was intended to meet the following objective performance specifications:

Set-on accuracy @ 50 ns:	±0.5 MHz
Frequency stability @ 50 μs:	±2.0 MHz
Input pulse power:	+15 dBm, ±1.5 dB
Power output:	+5 dBm

In addition to the set-on VCO assembly, three oscillators, which together cover the 11- to 18-GHz band and which use the gallium arsenide hyperabrupt diodes, were to be fabricated, demonstrated, and delivered. It was intended that these oscillators would be the same as required by the 11- to 18-GHz system and would meet the following objective specifications:

Frequency - Oscillator No. 1:	11.0 to 13.5 GHz
Oscillator No. 2:	13.5 to 16.0 GHz
Oscillator No. 3:	16.0 to 18.0 GHz
Output power:	+5 dBm min.
Input voltages:	+15 VDC @ 2.0 A max.
	±5 VDC @ 0.5 A max.
	120 VAC @ 2.5 A max.
Tuning voltage:	-1.0 V min to 30.0 V max

The material growth techniques for the hyperabrupt gallium arsenide varactor diodes were to be documented, and two sets of three suitably packaged

varactor diodes were to be delivered during the program. The objective specifications for these diodes were as follows:

Junction capacitance (@ 0 V):	1 $\pm$0.5 pF
Junction capacitance ratio:	8 to 10
Breakdown voltage:	30 V, min
Tuning slope (log C/log [V+1]):	1.0 min

The development of the hyperabrupt gallium arsenide varactors was intended to be a key feature of this program because of the enhanced linearity and reduced tuning voltage requirements of the voltage-controlled oscillators. Improvements to these parameters were considered necessary to meet the objective set-on accuracy and time. Enhanced linearity leads to improved accuracy because it reduces the need for corrections to match the frequency discriminator characteristic to the VCO tuning curve; set-on time is reduced by the lower tuning voltage swing because the slow rate limitations of the driver amplifier are reduced. These VCO characteristic improvements are provided by the use of hyperabrupt varactors as the variable capacitance tuning diodes because of the larger capacitance ratio this type of device offers in comparison with standard abrupt junction varactors. The larger tuning ratio is a result of the shaping of the dopant carrier concentration as a function of distance from the diode junction. RCA's controlled hydride vapor synthesis technique of growing gallium arsenide material is especially well suited for shaping the dopant profile, and during this program material was grown which produced diodes having exceptionally high capacitance ratios. A major difficulty encountered during this program which significantly degraded the actual VCO results was a dramatic reduction in varactor tuning ratio when rf power levels of the magnitude involved in transferred electron diode VCOs were applied to the hyperabrupt varactor. Considerable effort was applied toward determining the causes and correcting this problem.

The purpose of the set-on VCO system is to produce a microwave signal at the proper frequency for use in deceptive ECM systems as a replacement for existing TWT/delay line frequency memories. Because of the above-mentioned problem with the reduced tuning range when the hyperabrupt varactors were installed in oscillators, the 11- to 18-GHz set-on VCO system was not completed.

Data on the 8- to 11-GHz locked-open-loop VCO frequency memory system is included to describe the type of system performance which should be expected to result.

In addition to the number of sample varactor diodes which were delivered during the program, three J-band VCOs were fabricated and delivered to demonstrate the increased linearity and reduced tuning voltage swing which could be obtained. One of these VCOs demonstrated the capability to tune from 12.4 to 17.3 GHz with a nominally linear characteristic with less than a 15-V swing as compared with the severely nonlinear 40-V tuning voltage normally required using conventional abrupt junction varactors.

SECTION II

HYPERABRUPT VARACTOR VOLTAGE-CONTROLLED OSCILLATORS (VCOs)

A. USE OF HYPERABRUPT VARACTORS IN VCOs

The major incentive for the development of hyperabrupt varactors is the need for voltage-controlled oscillators with linear tuning characteristics and minimum tuning voltage swing. Presently, in systems which require linear tuning it is necessary to employ active linearizer circuits to compensate for the highly nonlinear tuning curve obtained when the standard abrupt-junction varactor diodes are used. Such linearizers cover a wide range of complexity depending upon the system requirements for linearity, bandwidth, tuning speed, modulation response, and available volume and power. In the more demanding applications, the linearizer becomes a large and costly item with numerous parts which tend to reduce system reliability.

RCA has previously completed a program to develop VCOs using hyperabrupt GaAs varactors (Contract No. N00039-74-C-0417). The major objective of this program was to develop hyperabrupt gallium arsenide varactors and demonstrate that improved VCO linearity would result from their use. It was expected that in many systems the improved linearity would be sufficient to eliminate the linearizer completely while in others the linearizer would be considerably reduced in complexity. Reduced tuning voltage swing was an objective because it is difficult to generate large tuning voltages with the fast rise times required in high tuning speed applications such as set-on VCOs.

For wideband applications, VCOs usually consist of an oscillator transistor or transferred-electron diode and the tuning varactor connected in a series arrangement as shown by the schematic diagram of Fig. 1. In this configuration for wideband tuning the capacitance of the varactor diode is a dominant parameter in determining the frequency of operation. The use of conventional abrupt-junction varactors, made from either silicon or gallium arsenide, results in a highly nonlinear frequency/voltage characteristic such as the typical X-band VCO tuning curve shown in Fig. 2 compared with a tuning curve obtained using a hyperabrupt varactor.

In addition to the effect of several second-order factors, this nonlinearity is a consequence of two major considerations, the first of which

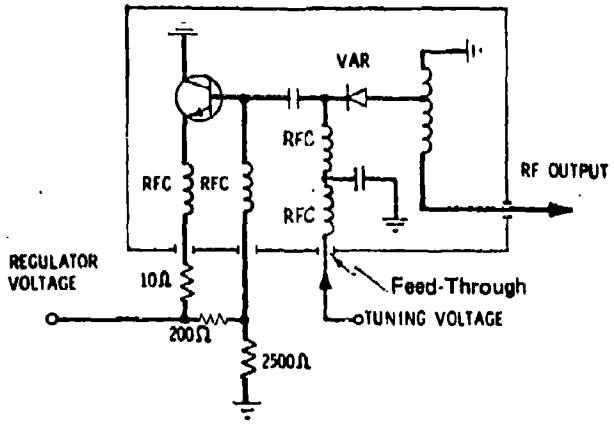

(a)

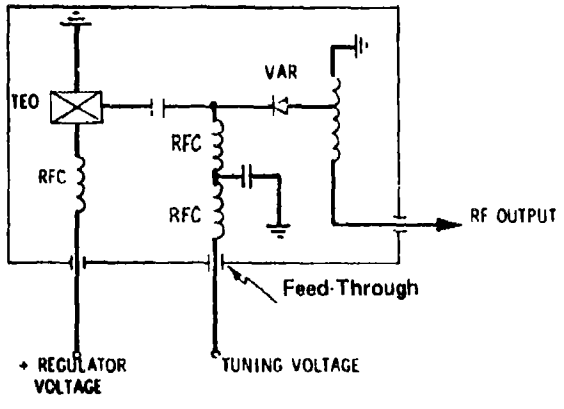

(b)

Figure 1. Schematic of (a) varactor-tuned transistor oscillator, and (b) varactor-tuned TEO.

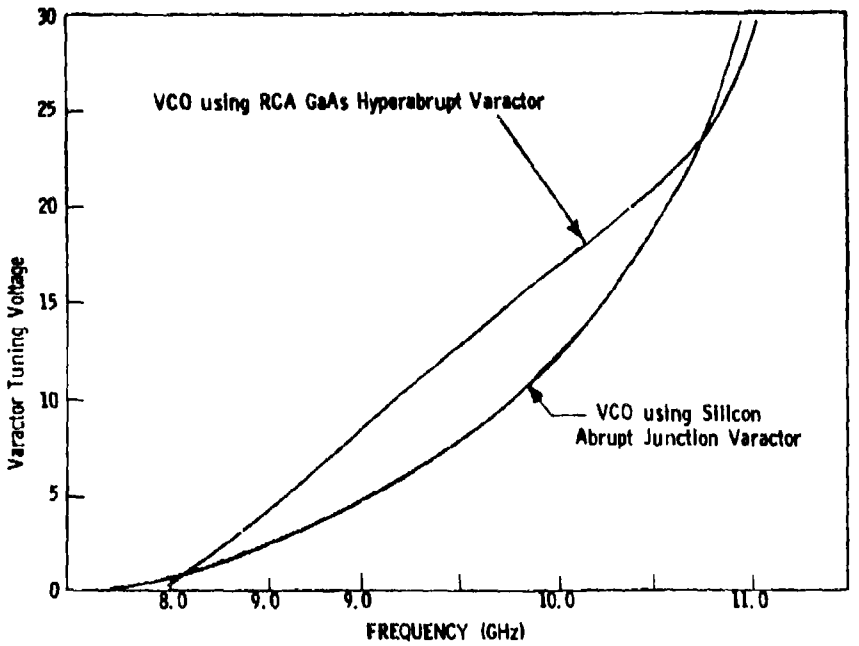

Figure 2. Comparison of tuning curves obtained with silicon abrupt junction varactors and RCA GaAs hyperabrupt varactors.

is simply that the resonant frequency in a series R-L-C circuit is not a linear function of capacitance but is related by the well-known basic expression:

$$f_o = \frac{1}{2\pi\sqrt{LC}} \tag{1}$$

which, for a circuit in which all elements other than the capacitance are fixed, reduces to:

$$f_o = K_1 C^{-.5} \tag{2}$$

The other major factor is the capacitance-voltage characteristic of the varactor. We can write the C/V law for a varactor as:

$$C_j = K(V + V_{bi})^{-\gamma} \tag{3}$$

By substituting this value for C in the resonant frequency expression of Eq. (2), a linear relation between tuning voltage and frequency results for the case of $\gamma = 2$. In practice, realization of such an idealized solution is prevented by several secondary factors which include:

(1) C_j is not the total capacitance of the circuit - there are strays, parasitics, and the output capacitance of the oscillator device.

(2) Other circuit inductances and capacitances are not independent of frequency because of transmission line effects.

(3) The output parameters of the oscillator device, transistor or TE diode, vary with frequency and loading.

Fabrication of tuning varactors which have a value of γ in excess of 0.5 requires the capability to control the doping density in the varactor junction region because the density must increase by a large factor over a distance of a few microns away from the junction. One of the best ways to achieve this result and the desired varactors with gallium arsenide is to use a gaseous phase epitaxial process in which the doping density is controlled by changing the flow rate of the doping gases while the material is being grown.

B. GENERAL CHARACTERISTICS OF TUNING VARACTORS

The physics of varactor diodes has been extensively studied and described in the literature [1]. We will quote the following results which are relevant to this discussion. The geometry under consideration, shown in Fig. 3, is a one-sided junction with the p^+ layer doped heavily compared to the n-layer, so that the depletion layer is entirely in the n-region. The p^+-n interface is assumed to be at $x = 0$ and doping density N is given by:

$$N = B\, x^m \tag{4}$$

1. S. M. Sze, *Physics of Semiconductor Devices*, (Wiley-Interscience, New York, 1969), pp. 114-116.

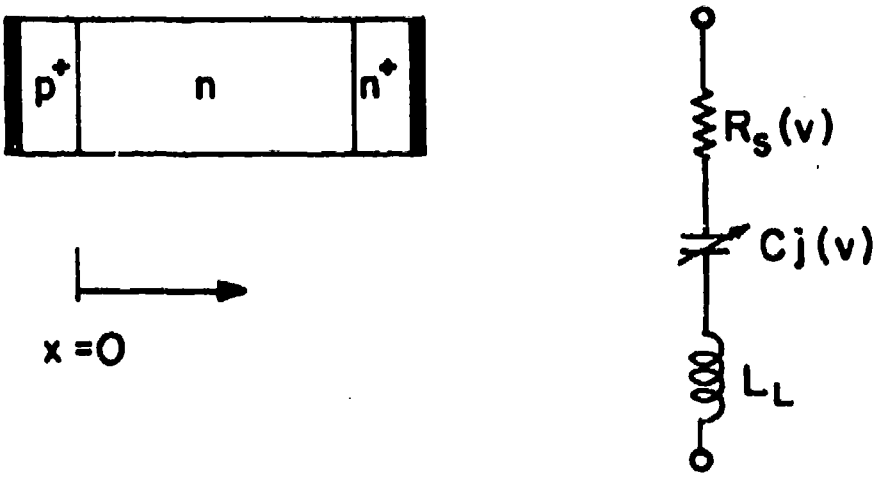

Figure 3. Geometry of abrupt p^+-n junctions.

For an abrupt junction, m = 0, and B = N_o. Under reversed bias conditions, the width of the depletion layer W is given by

$$W = \left[\frac{\varepsilon\ \varepsilon_o (m+2)(V+V_{bi})}{e\ B}\right] 1/(m+2) \tag{5}$$

where V is the applied reverse bias, V_{bi} is the built-in potential, and the other symbols have their usual meanings. The differential capacitance of the junction C_j is given by

$$C_j = A\left[\frac{e\ B\ (\varepsilon\ \varepsilon_o)^{(m+1)}}{(m+2)(V+V_{bi})}\right] 1/(m+2)$$

$$= A\left[\frac{e\ B\ (\varepsilon\ \varepsilon_o)^{(m+1)}}{(m+2)(V+V_{bi})}\right]^{\gamma} \tag{6}$$

where $\gamma = 1/(m+2)$.

For abrupt junctions: m = 0, γ = 0.5; for linearly graded junctions: m = 1, γ = 0.33; and for hyperabrupt junctions, γ is > 0.5, and ranges from 0.6 to 2. For simplicity, we will now specialize our discussion to the γ = 0.5 case, and look at the expressions for the junction capacitance ratio (JCR), and the varactor quality factor Q.

The junction capacitance ratio (JCR) is defined as the ratio between the zero bias capacitance and the capacitance when the depletion layer punches through to the n^+ substrate. We will assume an ideal device wherein the punch-through voltage V_p is equal to the breakdown voltage V_B. Using Eq. (6):

$$JCR = \left[1 + \frac{V_B}{V_{bi}}\right]^{1/2} \tag{7}$$

For a one-sided abrupt junction, the breakdown voltage V_B is given by the approximate universal expression [1]

$$V_B = 60 \left[\frac{E_g}{1.1}\right]^{3/2} \left[\frac{N_o}{10^{16}}\right]^{-3/4} \text{ volts} \tag{8}$$

where N_o is the background donor density and E_g is the bandgap. Thus, JCR increases with decreasing donor density. The usable capacitance ratio of the diode is less than JCR because of voltage-independent parasitic reactances such as the package capacitance.

The *figure of merit* of a varactor is given by the *quality factor Q(V)* or the *cutoff frequency* f_c. The cutoff frequency is defined as the frequency at which the quality factor is unity. At microwave frequencies, the varactor can be described by the series equivalent circuit of Fig. 3, and f_c is:

$$f_c(V) = \frac{1}{2\pi\, C_j R_s}\,; \tag{9}$$

f_c is a function of V since both C_j and R_s are a function of V, f_c increasing with increasing V. The package capacitance is neglected. The series resistance R_s can be separated into a bulk resistance R_b and contact resistance R_c. We then have the following expressions:

$$f_{c_b} = \frac{1}{2\pi\, C_j R_b} \quad \text{- Bulk cutoff frequency} \tag{10a}$$

$$f_{c_c} = \frac{1}{2\pi\, C_j R_c} \quad \text{- Contact cutoff frequency} \tag{10b}$$

and

$$\frac{1}{f_c} = \frac{1}{f_{c_b}} + \frac{1}{f_{c_c}} \tag{10c}$$

The bulk cutoff frequency can now be computed. Neglecting the very low resistances of the n^+ and p^+ layers, the series resistance R_b is the resistance of the undepleted part of the n-layer. Under our assumptions, the bulk cutoff frequency at zero bias, $f_{c_b}(0)$, is given by

$$f_{c_b}(0) = \frac{N_o e \mu}{2\pi \varepsilon_o [JCR-1]} \tag{11}$$

Using Eqs. (7) and (8), JCR for an abrupt junction is given by

$$JCR = \left[1 + \frac{K}{N_o^{3/4} V_{bi}}\right]^{1/2}$$

$$\text{where } K = 60 \left[\frac{E_g}{1.1}\right]^{3/2} .10^{12} \tag{12}$$

Equations (11) and (12) describe the basic tradeoff between JCR and f_{c_b}. Increasing N_o increases f_{c_b} but decreases JCR. Thus, if it is desired to increase f_{c_b} for a given JCR, it is necessary to use a semiconductor in which μ is high.

We can now compare Si and GaAs varactor performance based on the above framework. Figure 4 is a plot of the electron mobility at room temperature as a function of the effective donor density for both Si and GaAs. The curve for Si is taken from the literature, while that for GaAs is a plot of our own results. It is clear that in our region of interest the electron mobility in GaAs is five to six times that in Si. This higher mobility results in GaAs varactors having a higher cutoff frequency than Si varactors for a given donor density.

For tuning applications, however, it is the cutoff frequency as a function of JCR that is of prime importance. As is apparent from Eq. (7), JCR for an abrupt junction is a function of V_B/V_{bi}. Since the bandgaps of Si and GaAs are 1.12 and 1.41 eV, respectively, Si has slightly lower V_B than GaAs for a given N_o. V_{bi} for Si p-n junctions is around 0.7 V while that for GaAs is 1.0 V. As a consequence of these factors, for a given JCR, Si requires a slightly higher N_o than GaAs. This tends to slightly offset the mobility advantage of GaAs over Si. The difference in mobility, however, dominates, and

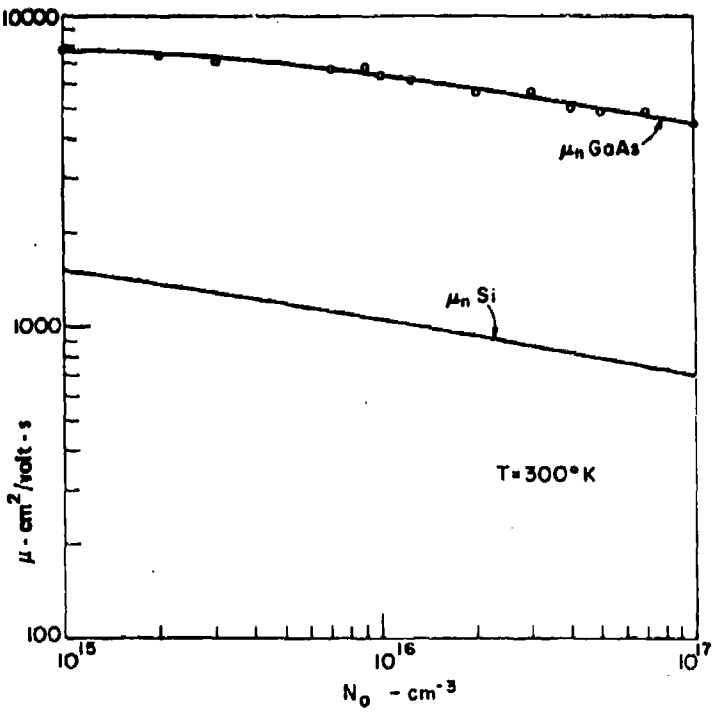

Figure 4. Room-temperature electron mobility in Si and GaAs.

GaAs p^+n junctions have about four times the cutoff frequency of Si p^+n junctions for a given JCR. If instead of GaAs p^+n junctions, GaAs Schottky barriers were used, we would have a V_{bi} of the order of 0.7 V, and the full advantage of the high electron mobility of GaAs could be taken. The choice between GaAs p^+n devices and Schottky barriers will be determined by cost and reliability tradeoffs.

In summary, GaAs varactors are superior in performance to Si varactors as a consequence of the electron mobility in GaAs being five to six times greater than that in Si. While some of the advantages are reduced because hyperabrupt varactors are inherently more lossy than abrupt junction varactors, the previously described linearity and reduced voltage advantages provided by the GaAs hyperabrupt varactors make the continued development of these devices essential for VCO set-on systems.

C. MATERIAL GROWTH AND PROCESSING TECHNIQUES

1. GaAs Epitaxy

Epitaxial GaAs is grown at RCA using the hydride vapor synthesis technique. This method has been extensively used to grow material for p^+-n abrupt junction varactors for parametric amplifier and UHF television tuners, p^+-n hyperabrupt varactors for microwave VCOs, p-n junction IMPATTs, TEDs, and high-performance GaAs power field effect transistors. The details of the hydride vapor process are well known [2] and will be discussed as relevant to this program. Figure 5 shows a schematic diagram of our system, and Fig. 6 is a photograph of a reactor which can handle substrates up to 5 cm in diameter.

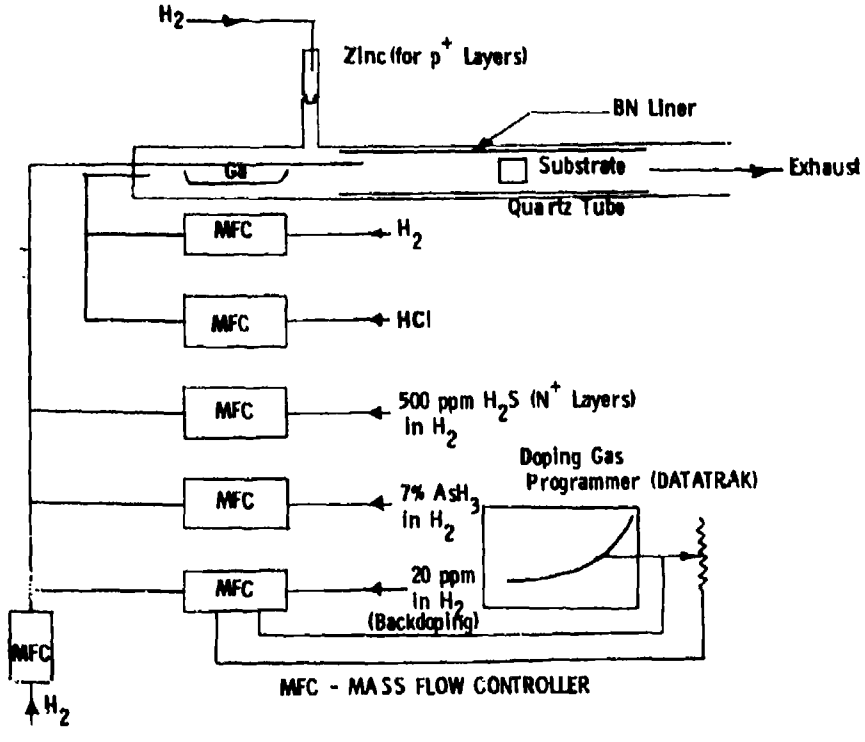

Figure 5. Schematic of vapor hydride system.

2. J. J. Tietjen, R. E. Enstrom, V. S. Ban and D. Richman, "Vapor-Phase Growth of Several III-V Semiconductors," Solid State Technology, pp. 42-49, (October 1972).

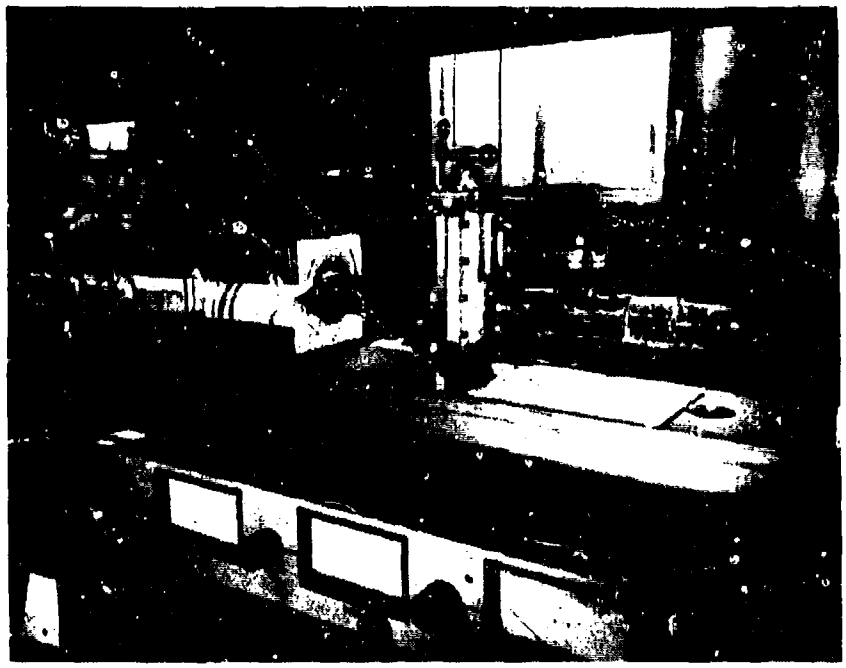

(a)

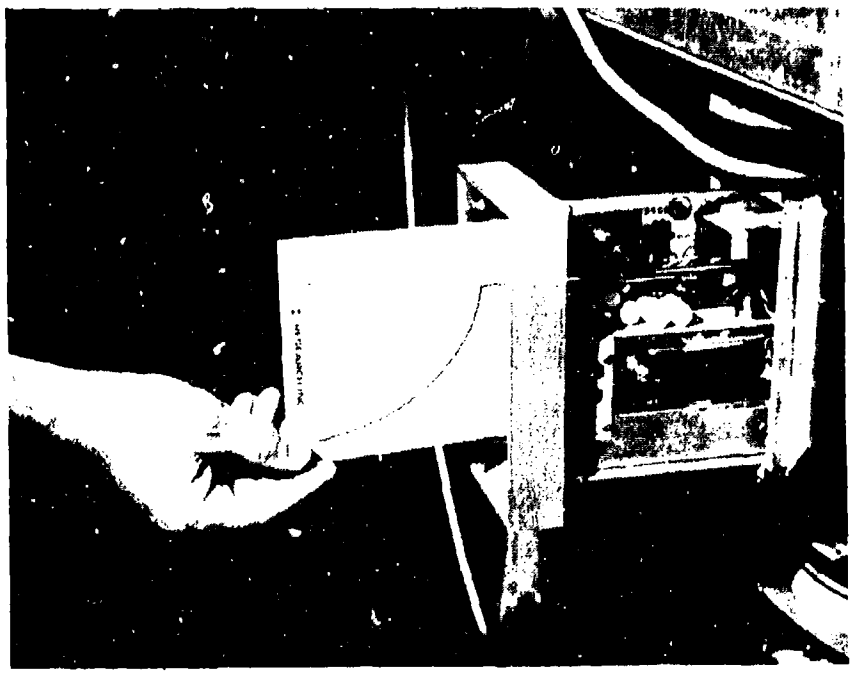

(b)

Figure 6. (a) Photograph of 2-in. bore reactor.
(b) Datatrak programmer for reactor.

The net donor concentration, N_D-N_A in GaAs produced by this method depends primarily upon the quality of the starting materials used; viz., AsH_3, HCl, and Ga. These starting materials are carefully chosen so that the background impurity density is in the 2 to 5 x 10^{14} cm^{-3} range. The required net donor concentration (8 to 12 x 10^{15} cm^{-3}) is obtained by controlled addition of a donor, S, introduced into the reactor as gaseous H_2S. This increases N_D-N_A by increasing N_D and thus results in less-compensated or higher-quality material. Our backdoping technique of adding controlled amounts of a known dopant is superior to the method of utilizing gases that happen to contain sufficient unknown impurities to bring the carrier concentration into the required range. This backdoping method, however, requires much more stringent control of the growth process.

All critical gas flows are regulated using electrically operated mass flow controllers (MFC). The mass flow through the MFC can be accurately controlled by applying an appropriate control voltage using either a potentiometer or a Datatrak analog programmer. The programmer is used to control the MFC in the backdoping 20-ppm H_2S line and this allows the growth of tailored n-doping profiles such as those required for hyperabrupt varactors. The reactor tube is made of quartz and has a high purity-pyrolytic BN liner. The BN liner prevents the SiO_2-HCl reaction and lowers the background doping and decreases the compensation ratio $[(N_D+N_A)/(N_D-N_A)]$.

One of the major advantages of the vapor hydride process is the ease with which controlled amounts of suitable gaseous doping chemicals can be introduced into the mainstream of the reacting gas. Suitable hardware exists to enable very accurate control of small gas flows. Figure 7 shows a plot of the doping concentration as a function of 20-ppm H_2S dopant flow for a large number of wafers. Figure 8 shows a typical hyperabrupt varactor profile. The Datatrak conductive card programmer was used for this growth run. The desired and actual doping profiles are shown in the figure.

Zinc is used as a dopant for the growth of p^+-layers. The method employed is to introduce a small container of zinc into a sidearm of the reactor that has an increasing thermal gradient along its length. The zinc-vapor concentration produced will provide the desired doping level. The zinc is carried into the main reactor tube by a flow of pure hydrogen.

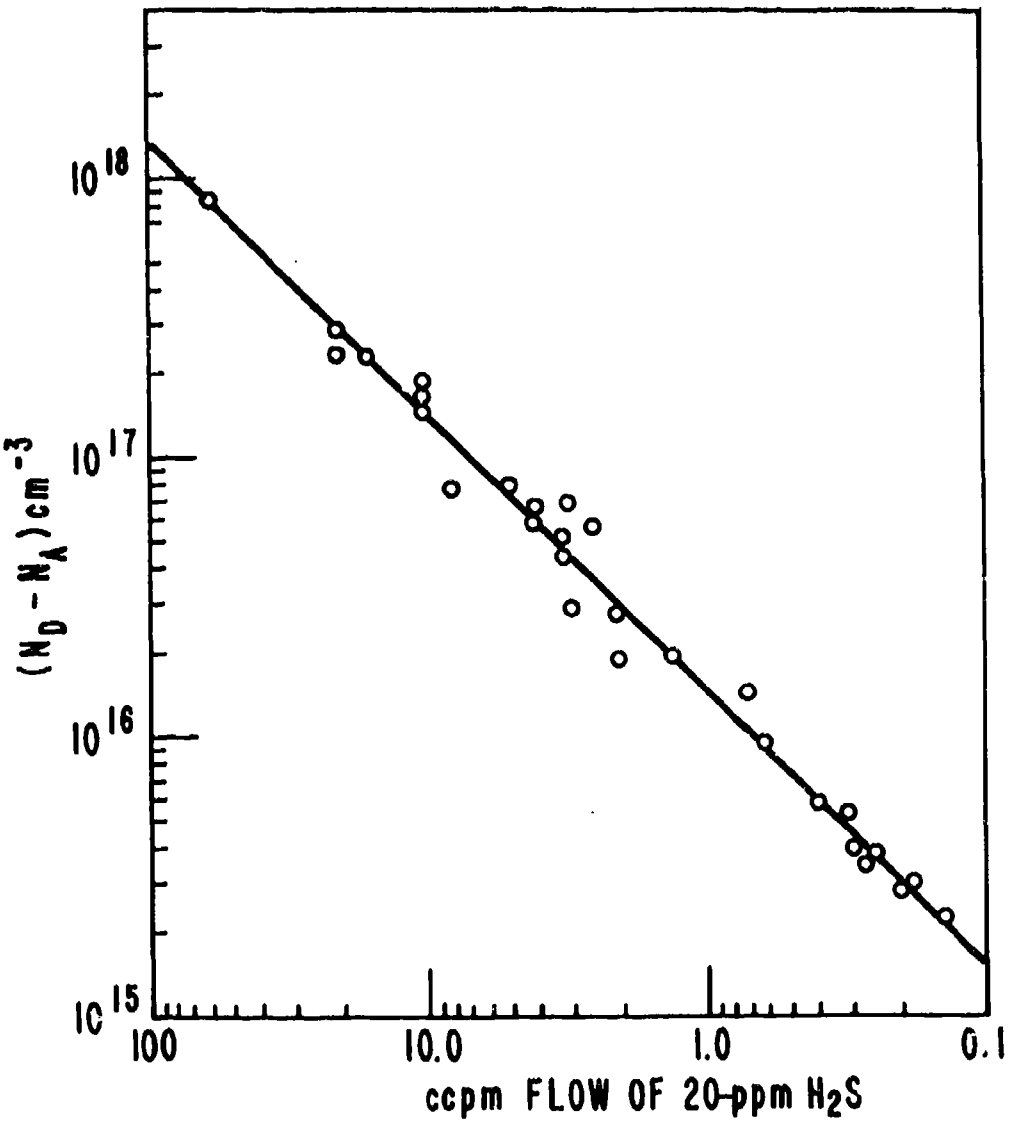

Figure 7. Plot of doping concentration as a function of 20-ppm H_2S dopant flow for a large number of wafers.

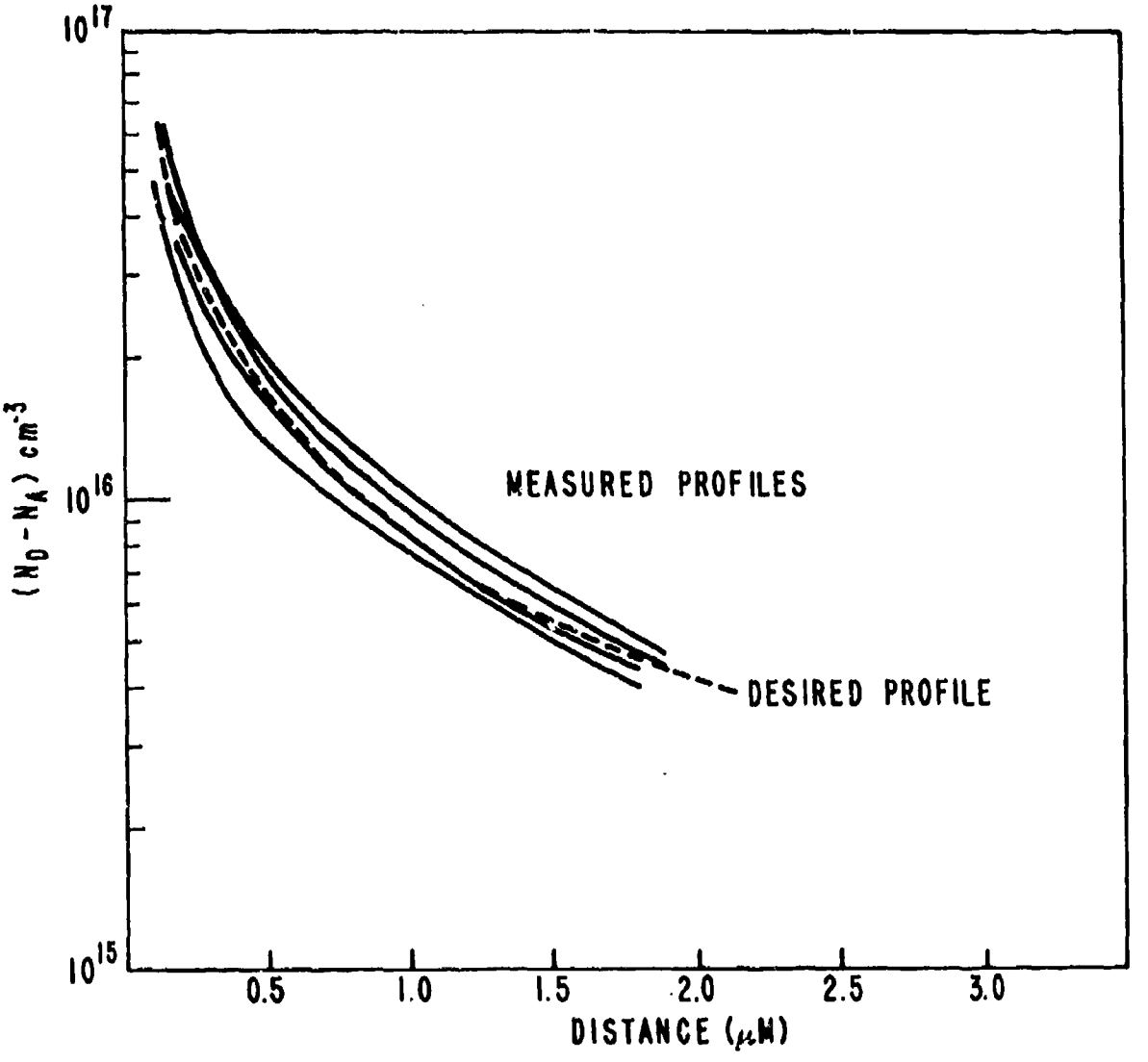

Figure 8. Profile of a typical hyperabrupt varactor.

One of the major advantages of the vapor-deposition system and backdoping techniques described is the ease with which they lend themselves to the sequential deposition of layers of varied doping types and concentrations. This is of significance in this program because the capability of producing sophisticated structures allows the realization of device performance otherwise impossible. Figure 9 is a scanning electron micrograph of a cleaved section through a wafer where n-, n^+-, n-, and p^+-layers have been sequentially deposited on a p^+-substrate. As will be described in a section on device technology, the growth of a varactor structure on a p^+- GaAs substrate allows us to use a self-limiting electrolytic etching technique for the fabrication of plated heat sink varactors for VCO applications.

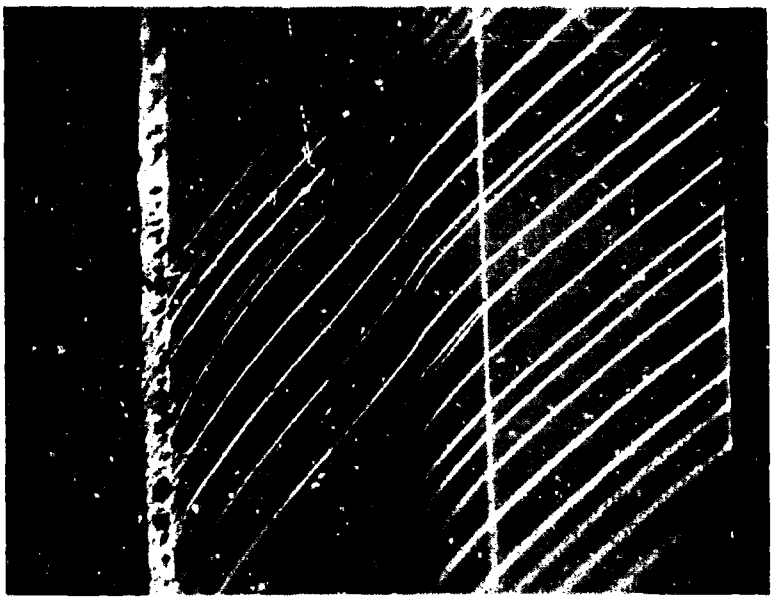

Figure 9. SEM of p^+-n-n^+-n-p^+ multilayer structure.

Figures 10 and 11 show the variation in doping profile of a typical 0.75 in. x 0.75 in. backdoped n-layer.

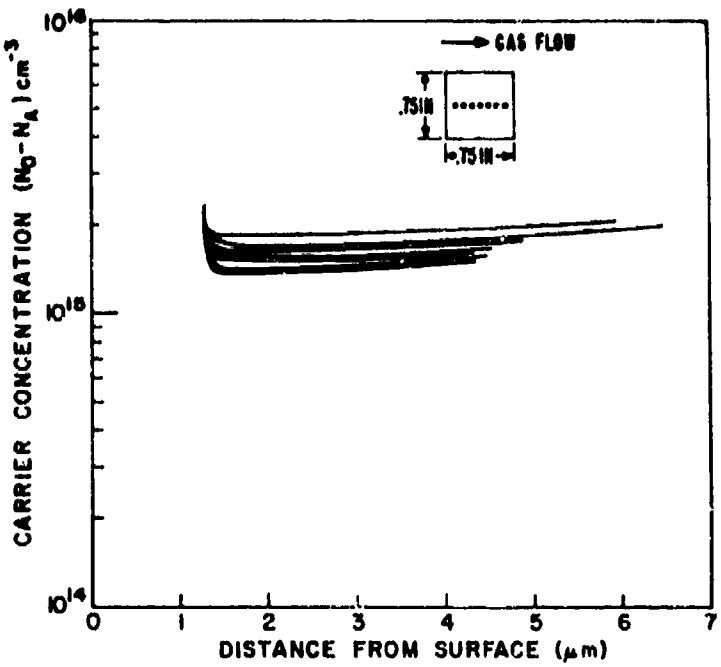

Figure 10. Impurity profile plots for Wafer No. 963 (side-to-side of substrate).

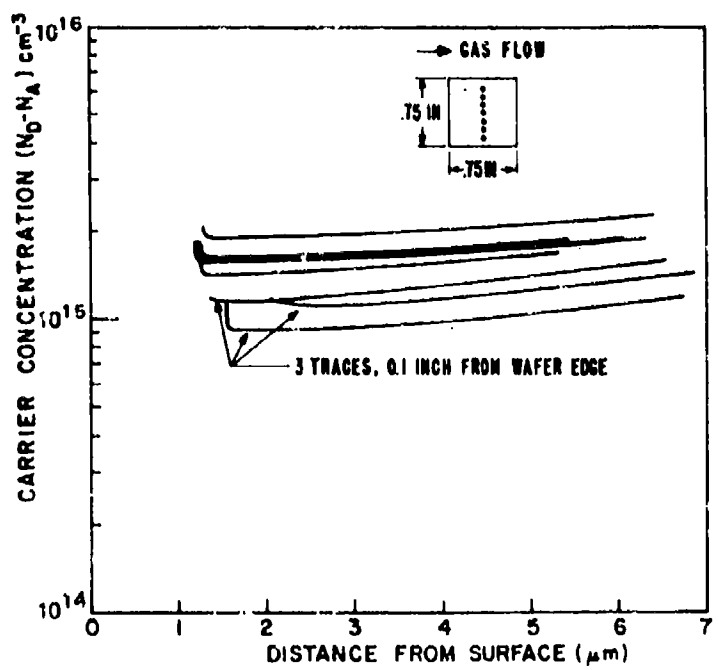

Figure 11. Impurity profile plots for Wafer No. 963 (top-to-bottom of substrate).

2. Varactor Fabrication

(a) Device Structural Concepts: - Conventional techniques used for producing mesa type diodes yield undesirable features in the device structure. These techniques employ etching of the grown epitaxial layers to produce mesas and retain a large portion of the underlying substrate in the finished device. The underlying substrate, which may be 100 to 150 μm thick and 250 to 500 μm in length and width, is used to provide a carrier for handling a mesa which may be only 75 μm in diameter and 10 μm thick and offers some mechanical rigidity for the relatively thin mesa.

The substrate offers a relatively high thermal resistivity (compared to copper or gold) and adversely increases the device thermal resistance, which in turn, increases post tuning drift. In addition, the relatively high electrical resistivity of the substrate (compared to copper or gold) offers a high electrical resistance which when compounded by skin effect at microwave frequencies serves to reduce the Q of the device.

During this program, RCA has evaluated the use of an integral heat sink in mesa type diodes in which the underlying substrate is replaced by an equally sized metal, either copper or gold. The metal heat sink then serves as the carrier for handling the device and provides the mechanical strength to support the mesa. Both the thermal and electrical resistivity are lower with the integral metal heat sink.

(b) Device Fabrication Technology: - The key to producing mesa type p-n junction diodes whose semiconductor layers consist only of those required to perform the desired electronic function, is the use of an etch technique which is highly selective as to p- or n-type material. The etch technique to be used is based on a method of electrolytically etching p^+-GaAs developed at the RCA Laboratories [3], and modified by workers at the Standard Telecommunications Laboratories, Ltd., Essex, England [4]. The method is highly selective in removing p-type material as opposed to properly doped n-type material.

3. C. J. Nuese and J. J. Gannon, "Electrolytic Removal of P-Type GaAs Substrates from Thin, N-Type Semiconductor Layers," J. Electrochem. Soc. 117, 8, 1094-1097 (1970).
4. E. J. Thursti, "A Method for Selective Substrate Removal from Thin P-Type Gallium Arsenide Layers," J. Phys. E, 7, 493-495 (1974).

This etching technique can be used very effectively in our process if the p-n varactor diode structure is grown on a p^+ substrate. An undoped n-layer (10^{14}-10^{15} cm^{-3}) is interposed between the substrate and the diode structure to act as both an etch "stopping" layer and as a buffer layer during growth to prevent any deleterious contamination of the diode layers due to the out diffusion of the p^+-substrate dopant.

The process flow chart for use with p^+-n_o-n^+-n-p^+ GaAs wafers to produce electrolytically etched varactor diodes with integral heat sinks is shown in Fig. 12. The basic steps are as follows:

(1) The bulk of the p^+-substrate upon which the desired semiconductor layers have been grown by epitaxial deposition from the vapor phase is reduced to approximately 200 μm by mechanical means.

(2) Deposition of ohmic contact on the p^+-face at a substrate temperature of 450°C.

(3) A 50 to 100-μm-thick Au heat sink is electroformed on this contact. This process is optimized to yield a stress-free heat sink.

(4) The p^+-substrate is then totally removed by electrolytic etching.

(5) The buffer n_o-layer is now removed by conventional chemical etching. Since this layer is only of the order of 3 μm thick, etch time control is simple and there is no loss of wafer parallelism. The total GaAs thickness is now of the order of 7 μm.

(6) AuGe:Au contacts are next evaporated on the n^+-layer through an appropriate mask to produce the desired metal dot diameter. This evaporation is done at low temperature to avoid thermal stress problems in the thin GaAs layers.

(7) A coating of photoresist is applied onto the metal dot pattern and developed by standard photolithographic techniques to yield a photoresist dot overlay on the metal dot pattern. The photoresist dot diameter exceeds the metal dot diameter to prevent undercutting of the metal dots during the mesa etch process.

(8) Device mesas are then defined by a spray-etching with a conventional chemical etchant.

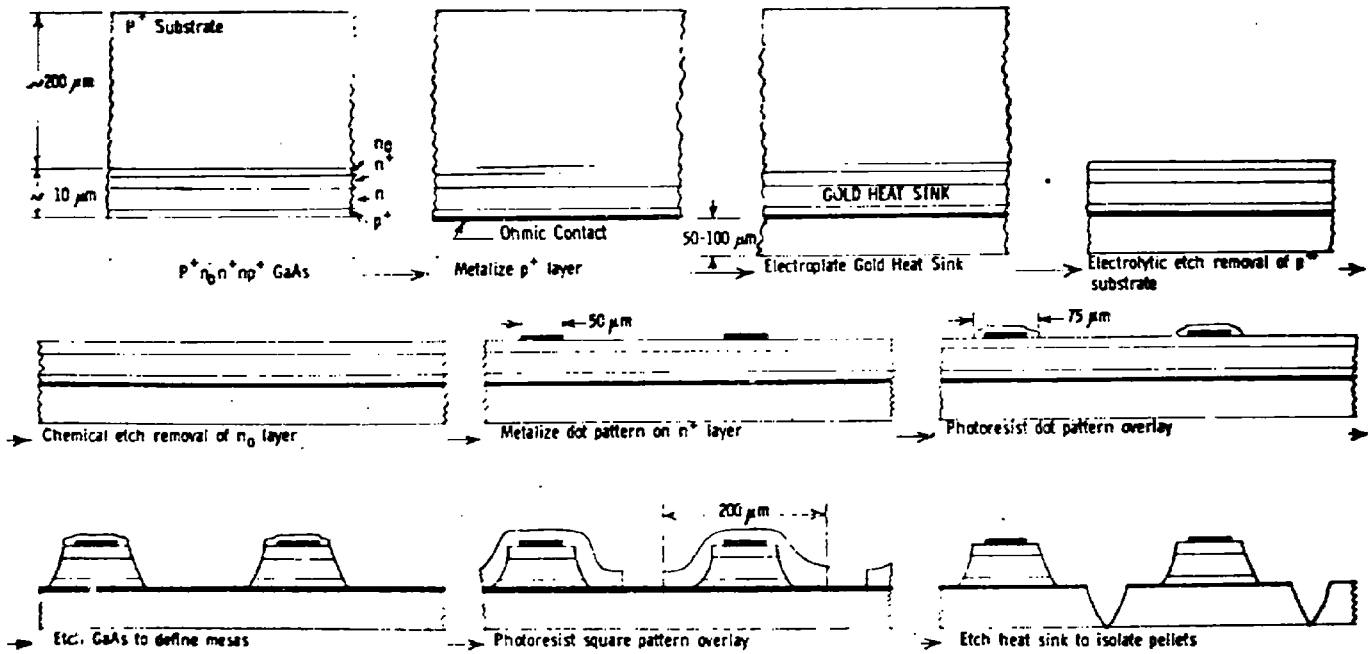

Figure 12. Fabrication flow chart for PHS GaAs varactors.

(9) The photoresist dot pattern is stripped off, and a second layer of photoresist is applied and developed to yield a 200-μm-square overlay on the etched mesa. The width of the channel openings between adjacent photoresist squares is approximately 50 μm.

(10) The heat sink is then etched in a conventional gold etchant to form isolated pellets.

A sketch of the electrolytic etch apparatus is shown in Fig. 13. The process used to remove the p^+ substrate from the n_o-buffer layer uses an electrochemical cell in which the sample to be etched forms the anode, a stainless

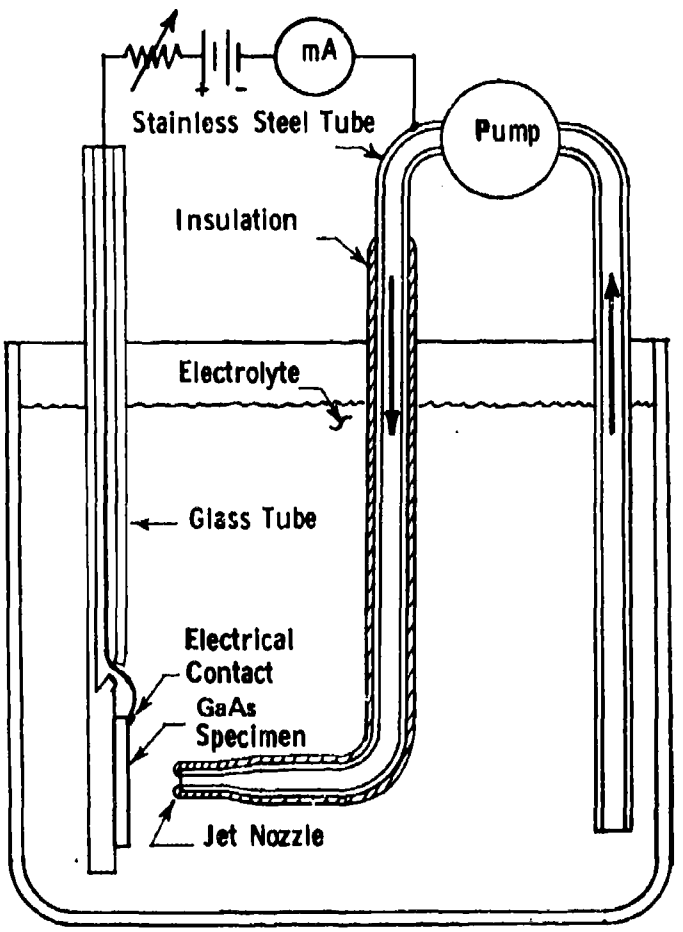

Figure 13. Electrolytic etch apparatus.

steel tube forms the cathode, and an aqueous potassium hydroxide solution is used as the electrolyte. Conduction is provided through the p^+-substrate via an ohmic contact on the p^+-substrate surface around the periphery of the wafer. The stainless steel tubing which forms the cathode of the cell is terminated in a jet nozzle which is positioned opposite the center of the fact of the GaAs specimen. To prevent areas of the disappearing substrate from becoming isolated from the ohmic contact it is desirable to promote rapid etching through to the buffer layer in the central region of the sample. This is accomplished by insulating most of the cathode from the electrolyte and leaving a small area exposed at the orifice of the jet nozzle opposite the GaAs anode. The resultant current crowding provides rapid etching opposite the cathode and allows the retreating substrate boundary to move outward toward the periphery of the wafer. A photograph of a partially etched wafer is shown in Fig. 14. The clearly defined circle in the center of the wafer marks the boundary of the p^+-substrate being removed and the n_o-buffer layer.

Figure 14. GaAs wafer partially processed in electrolytic etch. Photograph shows controlled selective removal of p^+ substrate after 30 minutes in etching tank. The surface within the clearly defined circle is the no-stop layer. The remaining p^+ substrate is the surface external to the circle.

The orifice diameter of the jet nozzle, the distance between the nozzle and the GaAs specimen, the etching current density, and the carrier concentration of the n_o-buffer layer have all been optimized to provide the desired controlled selective removal of the p^+-substrate.

The electrolyte is pumped through the system to provide a stream of ionized solution directed at the face of the wafer. The jet stream provides a scrubbing action at the face of the wafer and removes any sparingly soluble products of the etching which may build up on the face of the wafer and interface with the etch process.

A number of GaAs hyperabrupt varactor wafers have been grown and processed during the program which feature the integral heat sink and were processed by the electrolytic etch method. An SEM photomicrograph of one such hyperabrupt varactor is shown in Fig. 15. In this photograph, the total thickness of GaAs material is approximately 15 μm and the diameter of the metal contact on top of the mesa is 55 μm.

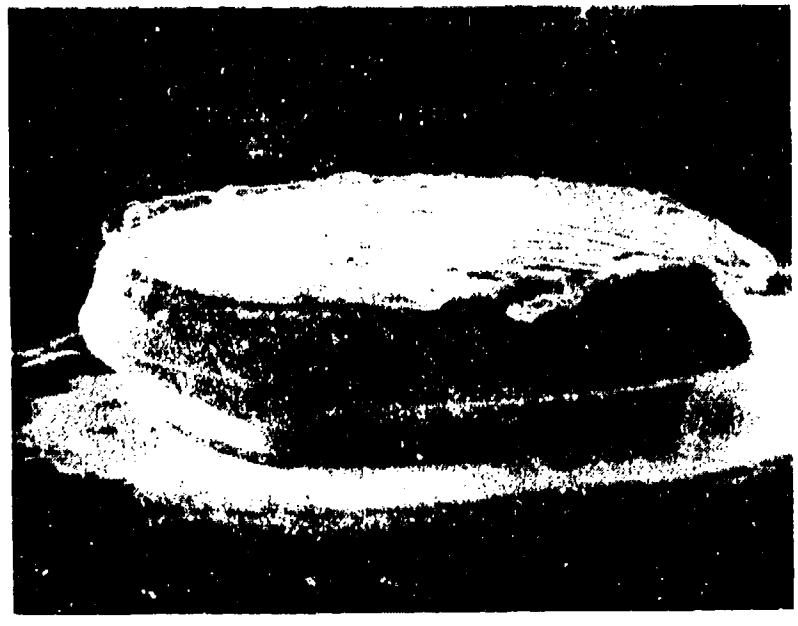

Figure 15. Copy of an SEM photograph of an integral heat sink type GaAs hyperabrupt varactor made with the electrolytic etch process. The total thickness of GaAs material is approximately 15 μm and the diameter of the metal contact on top of the mesa is 55 μm.

3. Varactor Evaluation

The varactors after fabrication go through two series of tests. The first series are measurements made at 1 MHz. The C/V characteristic and corresponding n/x curves are measured. The next series of tests is conducted at microwave frequencies and expected operating power levels. The latter tests are specially significant for VCO applications. We will describe our testing procedure and typical hyperabrupt GaAs varactor results.

(a) Low-Frequency Tests - The capacitance/voltage characteristic of varactor samples are measured at 1 MHz using a conventional capacitance bridge. These data are plotted on log-log paper to determine the γ of the varactors. Figure 16 shows C/V plots typical varactors from several wafers on log-log paper. Note that the γ for these wafers is about 0.63 which is slightly hyperabrupt.

Figure 17 shows a similar plot for devices from another wafer. Note γ of 0.7 over most of the tuning range. We have also plotted a computed "ideal" C/V curve for a 7- to 11-GHz VCO. The measured characteristic comes very close to the desired curve. Figure 18 is a C/V plot on linear graph paper. Note the capacitance ratio C(0)/(25) of 12.5 in contrast to about 5 for an abrupt junction. Tables 1 to 3 show capacitance/voltage data for GaAs hyperabrupt varactors mounted in AV159-4 micropill package and on 0.050 in. x 0.050 in. x 0.008 in. TiO_2 carriers. Figure 19 is a log C/log V plot from a recent wafer which has a γ of 0.8. Figure 20 shows the results of 2-GHz measurements on a packaged *abrupt* junction GaAs varactor. The cutoff frequency was measured using a precision holder and slotted line [5]. The junction capacitance was calculated from 2-GHz reactance data. Note that this device did *not* have a plated heat sink.

(b) Microwave Frequency Tests - During the course of our work with the hyperabrupt arsenide varactors, a number of VCOs were fabricated with varactors having exceptionally large capacitance ratios, and correspondingly wide frequency tuning ranges were expected. As will be discussed in a later section,

5. J. Collard, et al., *Microwave Semiconductor Diode Research*, Final Report, ECOM-0581-F, March 1969.

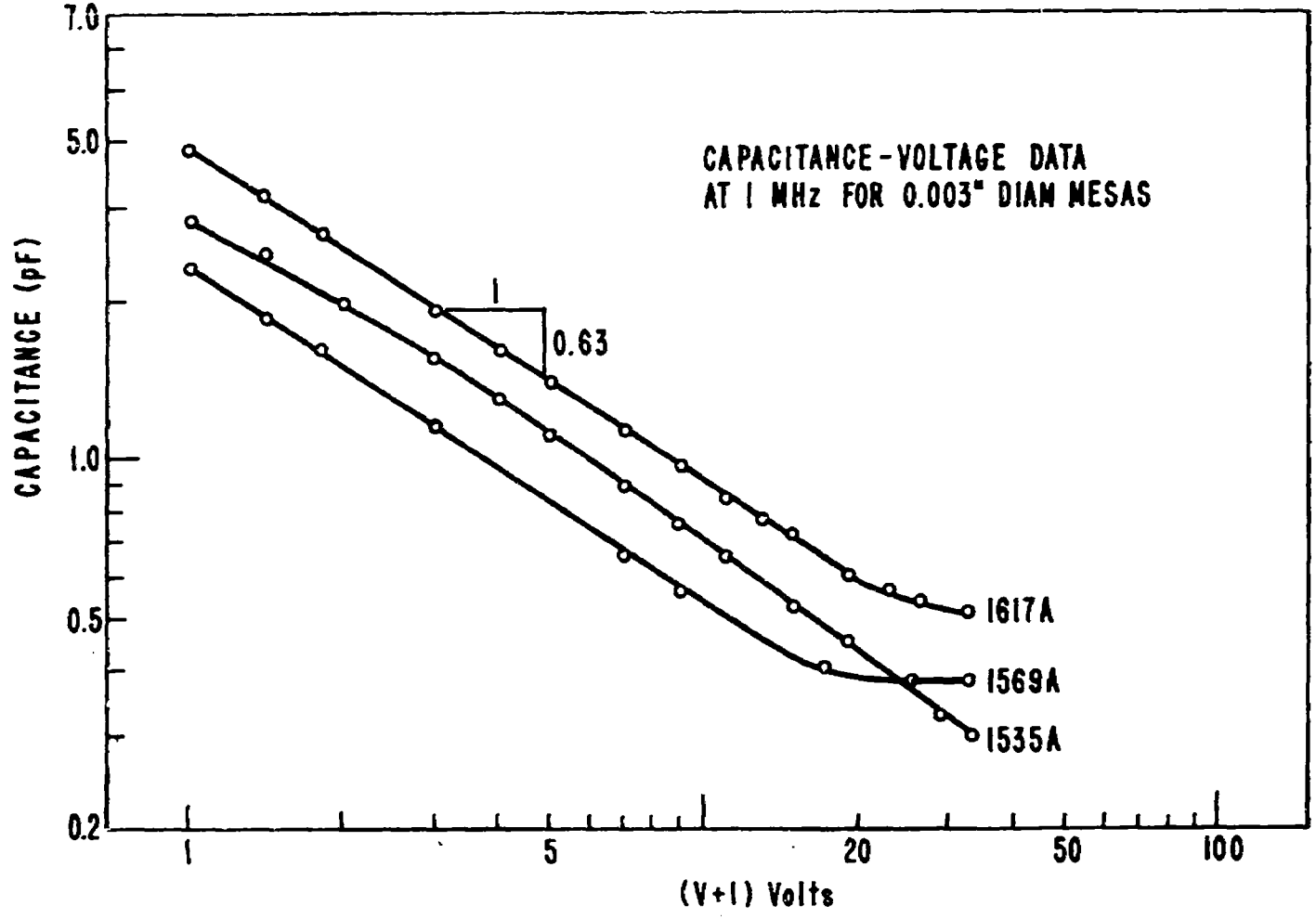

Figure 16. C/V characteristics of typical hyperabrupt GaAs varactors.

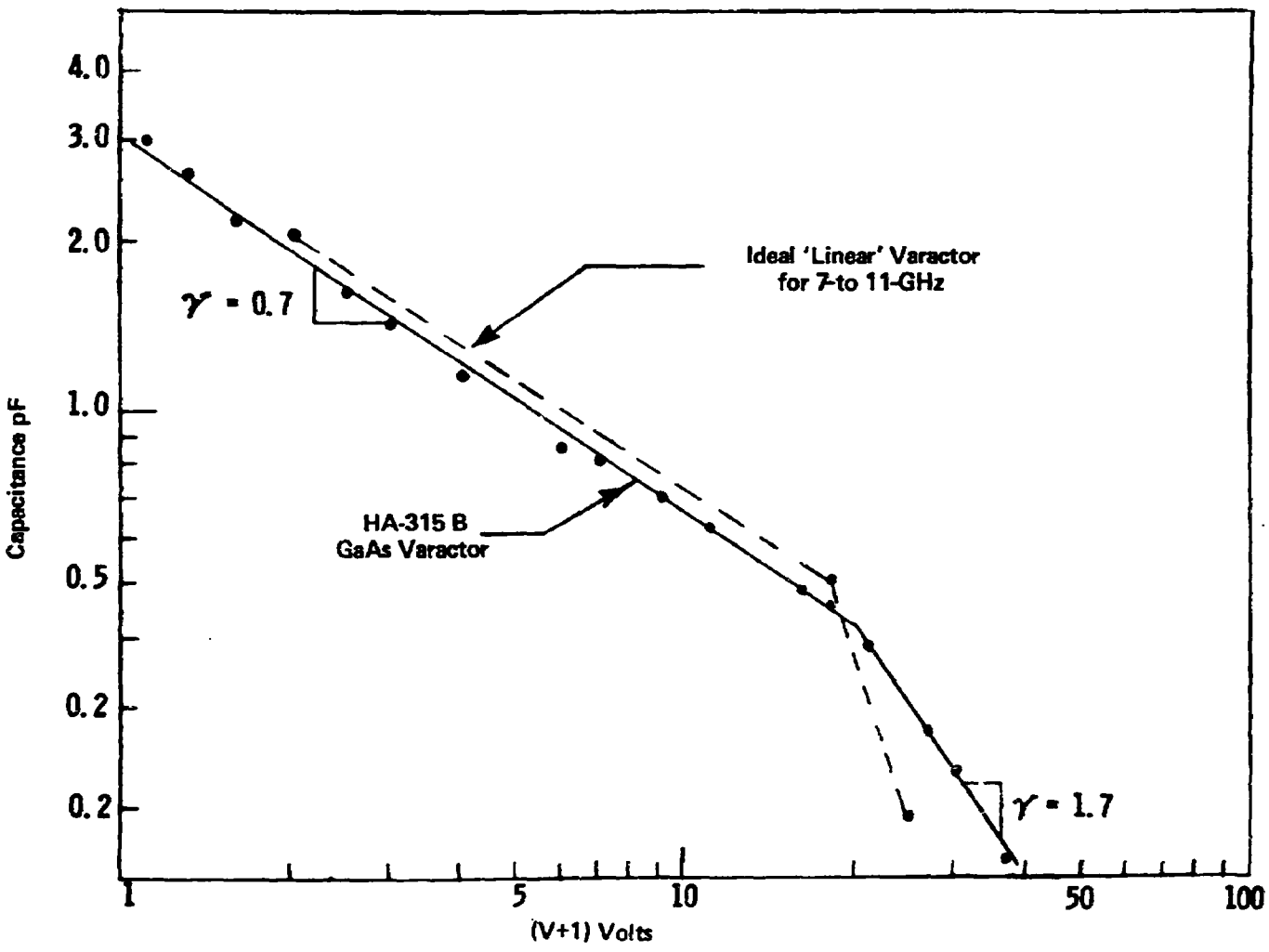

Figure 17. C/V characteristic of HA-315B GaAs varactor and computed C/V curve for ideal tuning varactor for RCA 7- to 11-GHz VCO.

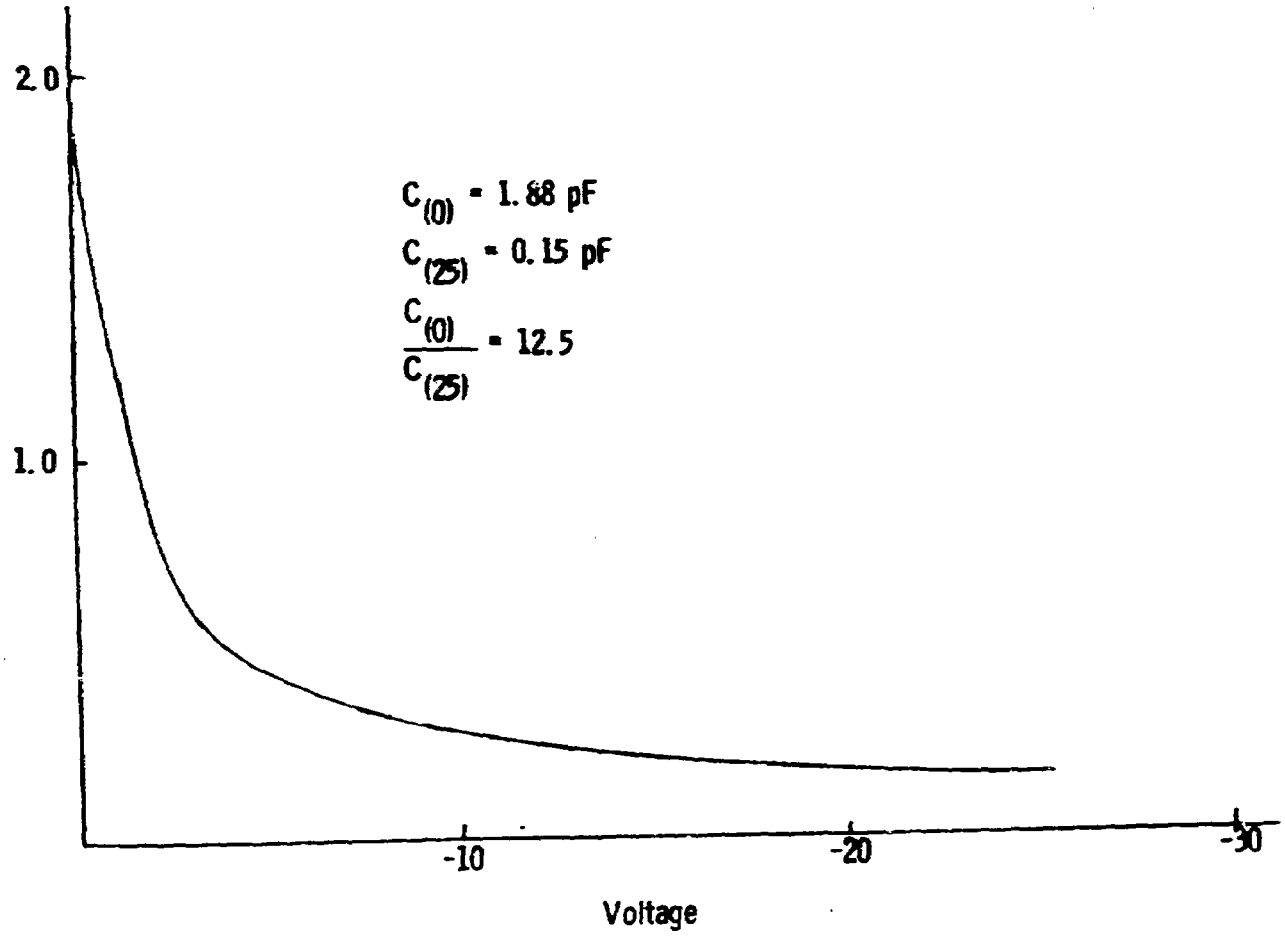

Figure 18. Unpackaged GaAs hyperabrupt varactor.

TABLE 1. CAPACITANCE OF HYPERABRUPT GaAs VARACTORS

Diode No.	Voltage in Volts												
	0	1	3	8	14	16	18	20	22	24	26	28	30
28	4.133	2.239	1.518	1.040	.827	.776	.727	.679	.630	.579	.523	.464	.398
29	4.053	2.223	1.503	1.024	.816	.768	.724	.683	.643	.602	.560	.516	.469
30	4.792	2.563	1.703	1.131	.847	.774	.707	.640	.575	.507	.435	(.358	.274)
31	4.284	2.324	1.556	1.058	.837	.786	.737	.690	.643	.594	.542	.487	.428
34	4.482	2.512	1.713	1.166	.901	.836	.775	.715	.655	.595	.529	.456	.372
36	4.273	2.368	1.594	1.082	.850	.795	.744	.695	.646	.597	.543	.489	.428
39	3.983	2.392	1.643	1.107	.844	.779	.719	.663	.609	.555	.500	.445	.386
41	4.815	2.578	1.743	1.188	.942	.885	.834	.787	.740	.694	.647	.596	.541
42	4.032	2.173	1.472	.998	.792	.745	.703	.665	.628	.591	.551	.513	.475
43	3.986	2.186	1.482	1.016	.811	.765	.724	.685	.647	.610	.573	.534	.495
26	5.737	2.757	1.828	1.189	.807	.692	.569	.409	(-.264	-.8	-1.068)		
16	3.931	2.268	1.578	1.095	.874	.820	.769	.717	.661	.601	.526	(-.055	-.130)
12	5.121	2.662	1.799	1.182	.804	.685	.561	.417	(.247	.032	-.251)		
11	3.857	2.243	1.525	1.018	.772	.712	.656	.599	.538	.445	(.006	-.339)	
22	5.820	2.681	1.761	1.136	.799	.705	.614	.519	.419	(.308	.184	.036	-.140)

TABLE 2. HYPERABRUPT VARACTOR - TYPE HV1001
MOUNTED ON 0.05 x 0.05 x 0.008 TiO_2 Carrier (C $\sim$ 5 pF)
CAPACITANCE (pF) vs REVERSE VOLTAGE (MESA NEGATIVE)

HV1001	-1	-2	-3	-4	-5	-6	-7	-8	-9	-10
V_{BD}(v)	55	64	60	40	50	58	58	55	55	50
I_R(μA)	30	80	80	50	20	125	35	100	20	10
V_j(V)	Capacitance (pF)									
0	6.17	6.20	6.24	6.28	6.57	6.42	6.26	6.42	6.23	6.26
-0.5	5.19	5.22	5.25	5.29	5.53	5.39	5.27	5.40	5.24	5.25
-1.0	4.52	4.59	4.60	4.66	4.85	4.73	4.63	4.74	4.59	4.60
-1.5	4.10	4.13	4.13	4.19	4.37	4.26	4.16	4.26	4.12	4.13
-2.0	3.75	3.77	3.76	3.84	3.99	3.89	3.80	3.90	3.76	3.76
-3.0	3.21	3.24	3.23	3.31	3.43	3.35	3.27	3.36	3.23	3.21
-4.0	2.84	2.87	2.85	2.93	3.04	2.96	2.86	2.97	2.84	2.82
-5.0	2.57	2.58	2.54	2.64	2.72	2.66	2.59	2.67	2.52	2.50
-6.0	2.30	2.31	2.24	2.40	2.43	2.37	2.31	2.39	2.24	2.20
-7.0	2.05	2.06	1.97	2.16	2.15	2.10	2.05	2.12	1.96	1.91
-8.0	1.81	1.82	1.72	1.93	1.88	1.85	1.81	1.87	1.71	1.66
-9.0	1.60	1.61	1.51	1.72	1.66	1.63	1.59	1.65	1.50	1.45
-10	1.39	1.41	1.31	1.52	1.46	1.44	1.41	1.48	1.32	1.25
-15	0.78	0.79	0.73	0.86	0.80	0.79	0.78	0.81	0.72	0.69
-20	0.50	0.50	0.48	0.56	0.53	0.50	0.49	0.52	0.47	0.46
-30	0.38	0.39	0.41	0.41	0.43	0.40	0.40	0.40	0.41	0.41

Gamma equals 1.55 for V_j = -9 to -20 volts (1.6 to 0.5 pF)
Gamma equals 0.5 for V_j = Zero to -5 volts (6.2 to 2.6 pF)

TABLE 3. HYPERABRUPT VARACTOR - TYPE HV1000
MOUNTED IN AV-159-4 MICRO-PILL PACKAGE (C $\sim$ 0.3 pF)
CAPACITANCE VS REVERSE VOLTAGE

HV1000	-36	-39	-41	-42	-43
V_{BD} (V)	36	35	38	46	45
I_R(μA)	100	100	100	100	100
V_J(V)	Capacitance (pF)				
0	4.27	3.98	4.81	4.03	3.99
-1	2.37	2.39	2.58	2.17	2.19
-3	1.59	1.64	1.74	1.47	1.48
-8	1.08	1.11	1.19	1.00	1.02
-14	0.85	0.84	0.94	0.79	0.81
-16	0.79	0.78	0.88	0.74	0.76
-18	0.74	0.72	0.83	0.70	0.72
-20	0.69	0.66	0.79	0.66	0.68
-22	0.65	0.61	0.74	0.63	0.64
-24	0.60	0.55	0.69	0.59	0.61
-26	0.54	0.50	0.65	0.55	0.57
-28	0.49	0.44	0.60	0.51	0.53
-30	0.43	0.39	0.54	0.47	0.49

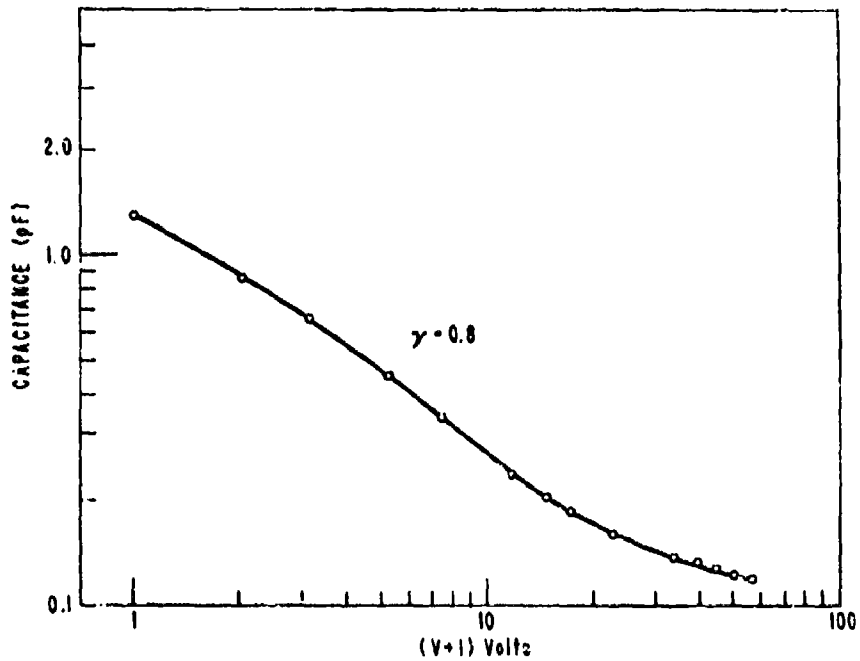

Figure 19. C/V characteristic of PHS GaAs hyperabrupt varactors from recent wafer.

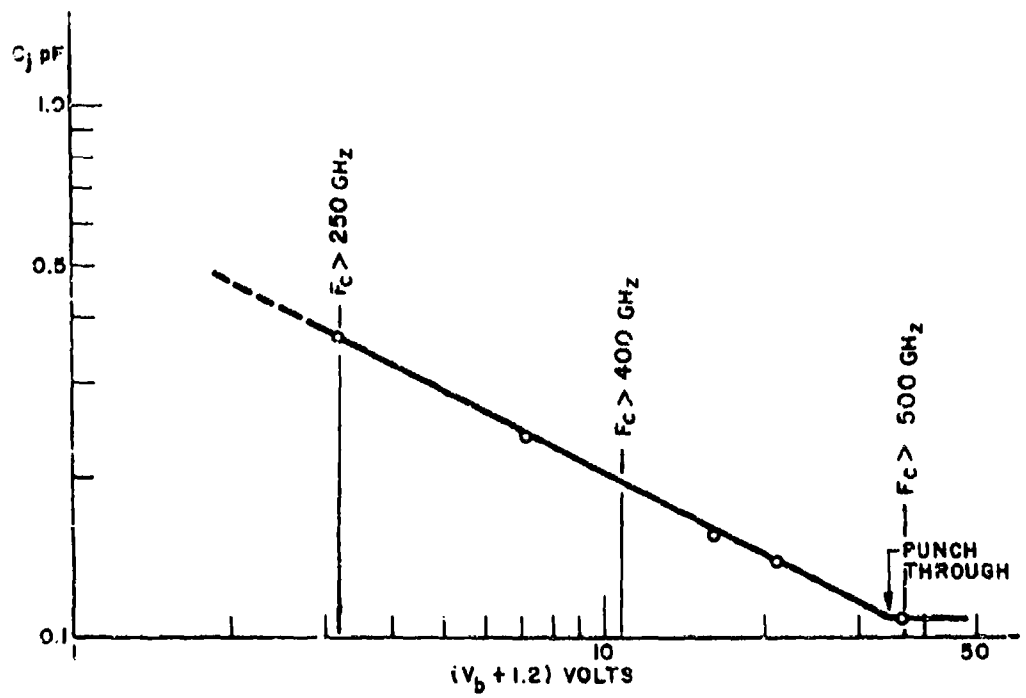

Figure 20. Capacitance and cutoff frequency of a GaAs p-n junction varactor measured at 2 GHz. (Device did not have plated heat sink.)

this was not often the case, and in an attempt to determine the cause, special network analyzer impedance measurements were made at X-band frequencies of the varactors as a function of applied tuning voltage and power level. Figure 21 is an example of the results obtained from a conventional silicon abrupt junction varactor. As may be observed, there is virtually no difference in the impedance shift with tuning voltage at applied power levels from 12 to 400 mW; in fact, there is a slight increase at the higher power level due to the normal capacitance offset caused by averaging of the rf signal voltage swing across the nonlinear varactor C/V characteristic. The measurement technique provides a means of assaying the effect of impressed rf power level on the impedance/voltage characteristic which at a given frequency can be reduced to the C/V characteristic of the varactor being tested.

D. HYPERABRUPT VARACTOR DIODE CHARACTERISTICS

One requirement of the contract was the delivery of two sets of three each hyperabrupt gallium arsenide varactors. The first group was delivered in December, 1975, and consisted of plated heat sink varactors from Wafer No. 1569. Test data are shown in Table 4. The C/V characteristic of an unpackaged device from the same group is plotted in Fig. 22. As may be seen, values of $\gamma = 0.8$ were measured over a substantial region of the tuning curve and a C_o/C_{20} capacitance ratio of 7.7:1 was obtained.

A second group of three packaged devices was delivered in July, 1976. The test data are shown in Table 5. An average capacitance ratio of approximately 3:1 was obtained with a 0- to 15-V reverse-bias voltage swing. Of course, a larger ratio was obtained with a 40-V swing but an objective of the hyperabrupt varactor program was to facilitate wideband tuning with a small voltage swing. The fixed package capacitance of 0.29 pF was included in these measurements and reduced the capacitance ratio significantly. For example, Varactor #7 had a 0- to 15-V capacitance ratio of 3.3:1 after packaging; without the package, the capacitance ratio would have been 8.7:1.

A number of other wafers were grown using the described process, some conventionally mounted and some with plated heat sinks. Data on a large number of varactor diodes were previously shown in Tables 1, 2, and 3. Some extremely large tuning ratios were obtained from a series of hyperabrupt varactors grown

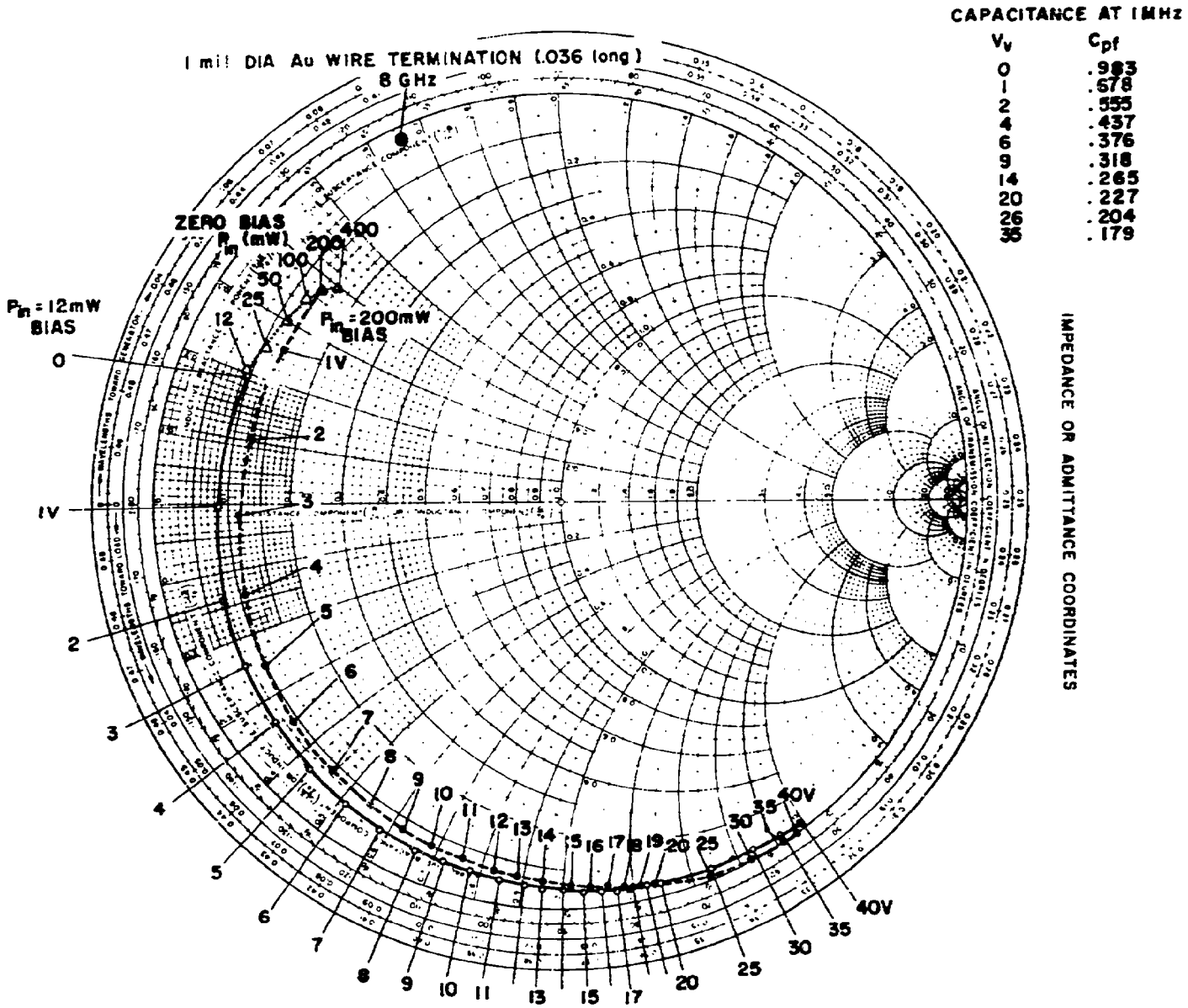

Figure 21. Smith chart plot of varactor impedance as a function of bias and input power at 8 GHz.

TABLE 4. GALLIUM ARSENIDE HYPERABRUPT VARACTOR

Polarity: Reverse polarity, flange positive.
Package Type: AV159-4 Package Capacitance: 0.29 pF

Serial Number		2	4	5
V_{BD}	volts	58	60	57
I_R	μA	< 1	< 1	< 1
C_o	pF	1.527	1.457	1.385
C_1		1.146	1.089	1.022
C_2		0.962	0.911	0.857
C_4		0.771	0.729	0.688
C_6		0.670	0.634	0.598
C_{10}		0.566	0.539	0.509
C_{15}		0.514	0.494	0.464
C_{20}		0.490	0.474	0.445
C_{30}		0.467	0.455	0.427
C_{40}		0.456	0.444	0.419
C_o/C_{15}		2.97	2.95	2.93
C_oC_{20}		3.12	3.07	3.05
C_o/C_{30}		3.27	3.20	3.18
C_o/C_{40}		3.35	3.28	3.24

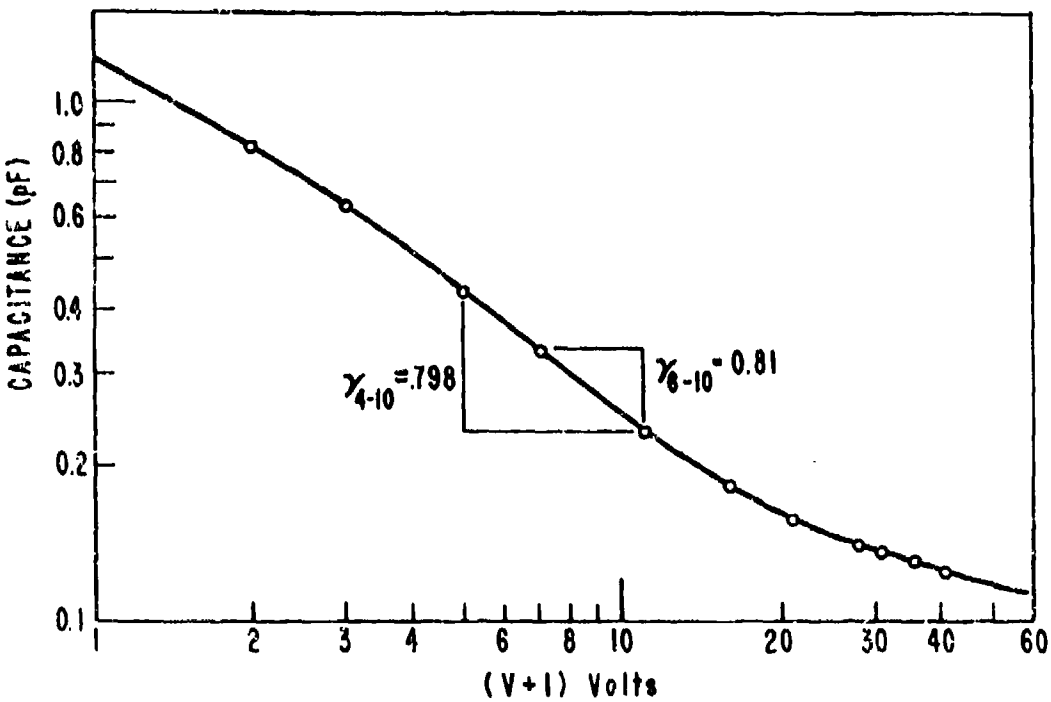

Figure 22. GaAs hyperabrupt varactor C/V curve.

subsequent to the plated heat sink work. These varactors were processed as Schottky-barrier devices. Some typical data are shown in Table 6. Diodes from both these wafers, B408 and B410, were subsequently used to fabricate VCOs. Figure 23 shows the C/V characteristic of one 0.010-diameter dot on the unetched wafer. As may be observed, a value of $\gamma = 2$ was obtained at the high voltage end of the tuning range.

E. VOLTAGE-CONTROLLED OSCILLATORS

A number of voltage-controlled oscillators were built using tuning diodes from several of the hyperabrupt gallium arsenide varactor wafers evaluated during this program. Although the end purpose of the program was to develop varactors suitable for 11- to 18-GHz VCOs, the varactor diodes were evaluated in oscillators at frequencies from 2.5 to 18.5 GHz, and these results will also be described. Since the basic design work on the frequency memory system was done on Contract No. N00039-74-C0227 for the 7- to 11-GHz frequency band,

TABLE 5. GALLIUM ARSENIDE HYPERABRUPT VARACTOR

Polarity: Reverse polarity, flange positive.
Package Type: AV159-4 Package Capacitance: 0.29 pF

Serial Number		6	7	8
V_{BD}	volts	55	60	58
I_R	μA	< 1	15	< 1
C_o	pF	1.214	1.369	1.475
C_1		0.927	0.999	1.098
C_2		0.787	0.822	0.915
C_4		0.642	0.642	0.727
C_6		0.565	0.549	0.630
C_{10}		0.485	0.547	0.532
C_{15}		0.442	0.413	0.485
C_{20}		0.432	0.389	0.464
C_{30}		0.407	0.378	0.444
C_{40}		0.398	0.369	0.433
C_o/C_{15}		2.75	3.31	3.04
C_o/C_{20}		2.81	3.52	3.18
C_o/C_{30}		2.98	3.62	3.32
C_o/C_{40}		3.05	3.71	3.41

TABLE 6. CAPACITANCE (pF) of 0.010"-DIAMETER SCHOTTKY BARRIERS

Tuning Voltage (V_{dc})	Wafer B408			Wafer B410	
	#1	#2	#3	#1	#2
0	75.3	72	82.3	46.5	49
1	-	38.8	41	23.6	-
2	-	26.4	28	12.4	-
3	-	20	22	6.4	-
4	-	15	16.5	4.7	-
5	-	11	11.6	3.9	4.2
6	-	8	7.1	3.4	-
8	-	5.2	4.5	2.7	3.0
10	4.1	3.3	-	2.4	2.5
12	3.4	4.2	-	2.4	2.4
14	3.1	-	-	2.3	2.3
16	2.6	-	-	-	-
18	2.4	-	-	-	-
20	2.5	-	-	-	-
	$C_o/C_{20} = 30$	$C_o/C_{12} = 17$	$C_o/C_8 = 18$	$C_o/C_{14} = 20$	$C_oC_{14} = 21$

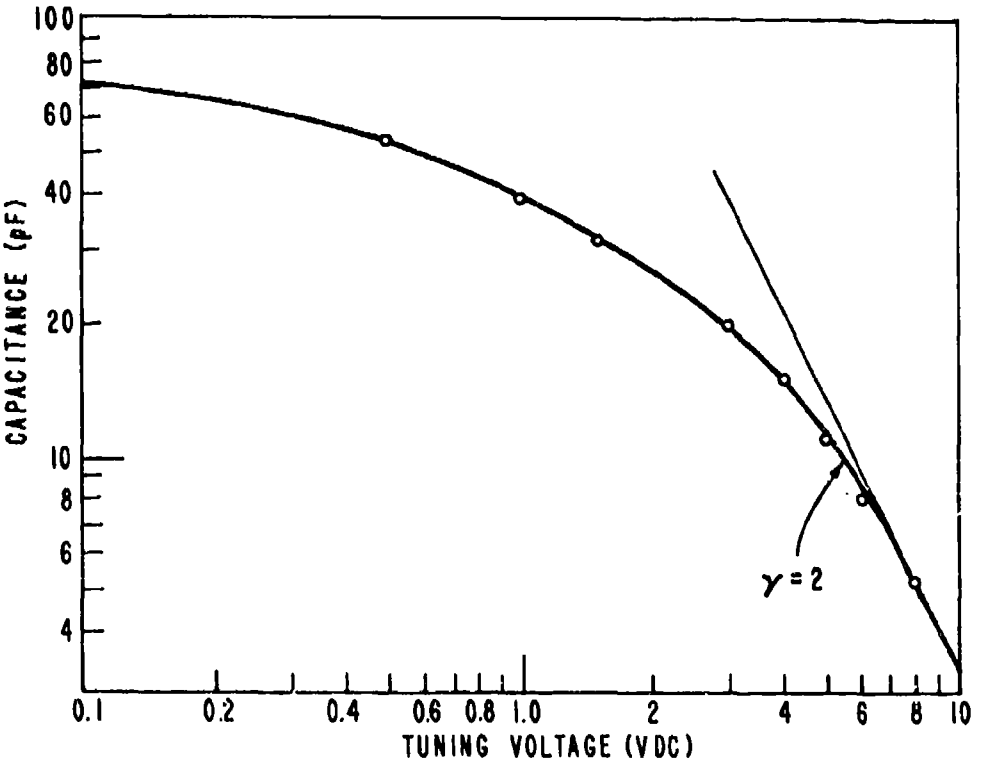

Figure 23. C/V characteristic of unetched hyperabrupt varactor No. 408 (0.01" dots).

considerable effort was directed at evaluating VCOs covering this range and most of the earlier-mentioned difficulties in obtaining oscillator bandwidths commensurate with the varactor capacitance ratios were noticed during this work. This problem will also be discussed in this section.

Delivery of three VCOs to cover the 11- to 18-GHz frequency band in three nominally linear, low-voltage tuning frequency segments was a requirement of the program. The frequency and output power performance curves of these three VCOs, which were delivered in April, 1976, are shown in Figs. 24(a), 25(a), and 26(a). The first of the three oscillators was tunable from 11 to 13.5 GHz with a tuning voltage swing of 0 to 22.5 V and was linear to within approximately 30 MHz from 11.5 to 13.56 GHz. This linearity is within the limits of some receiver type specifications for VCOs which have previously required complex linearizers. The particular VCO design used for this band nominally covers a slightly greater range (11 to 14 GHz) with about the same voltage swing, but

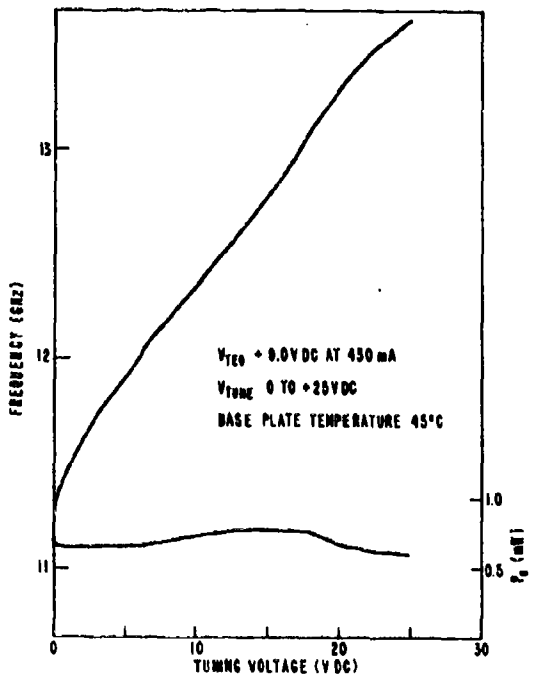

(a)

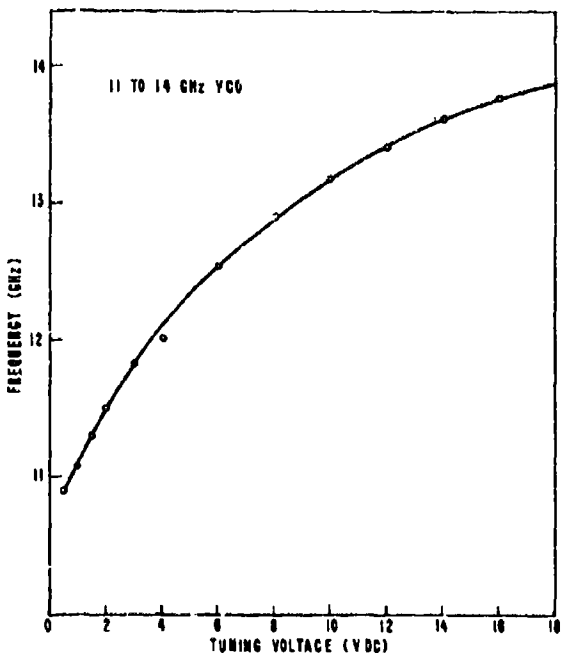

(b)

Figure 24. (a) Low band VCO with GaAs hyperabrupt varactor.
(b) Low band VCO with GaAs conventional varactor.

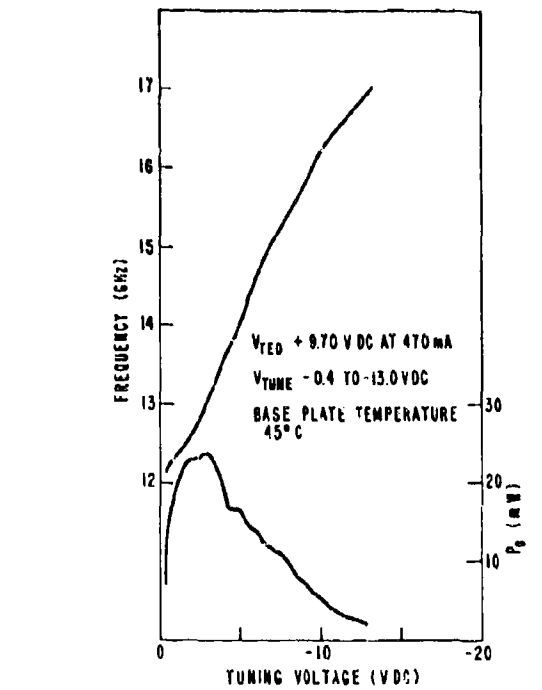

(a)

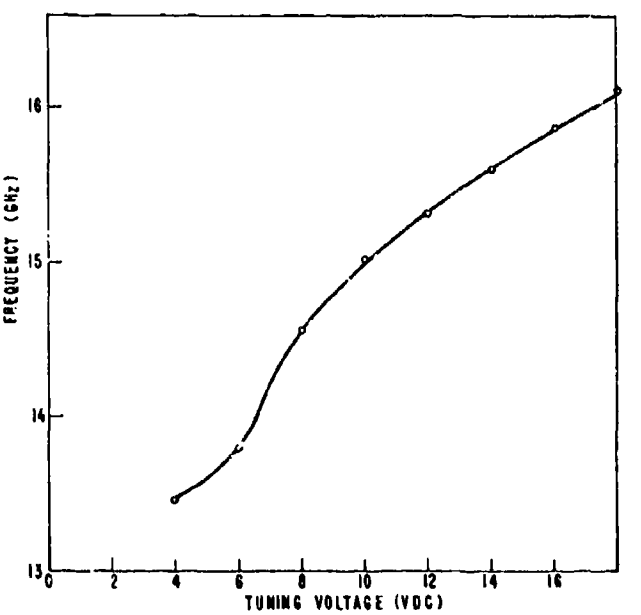

(b)

Figure 25. (a) Mid-band VCO with GaAs hyperabrupt varactor.
(b) Mid-band VCO with GaAs conventional varactor.

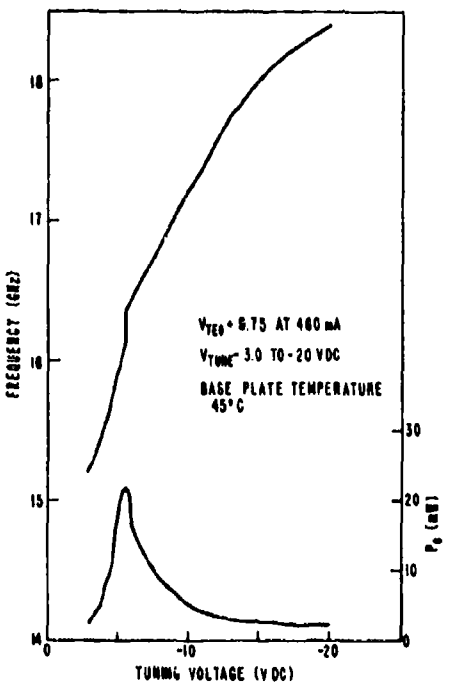

(a)

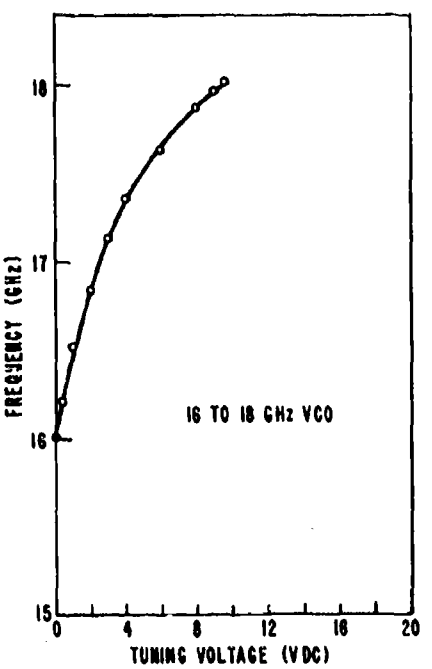

(b)

Figure 26. (a) High band VCO with GaAs hyperabrupt varactor.
(b) High band VCO with GaAs conventional varactor.

with a tuning curve having the characteristic shown in Fig. 24(b), the tuning curve of the same oscillator using a conventional GaAs varactor. The improved linearity performance was obtained using a conventional heat sink hyperabrupt varactor from Wafer 1334 for this oscillator, and the previously reported reduction of capacitance at the low end is believed responsible for the less than anticipated tuning range.

Better performance was obtained from the second of the three oscillators as shown by Fig. 25(a), particularly when compared with the typical tuning characteristic of the same oscillator using conventional GaAs varactors as shown by Fig. 25(b). Instead of the limited coverage of 13.5 to 16 GHz, the VCO using a plated heat sink hyperabrupt varactor from Wafer 1569 covered a frequency range of 12.5 to 17 GHz in about 12 V with a departure from linear of about 100 MHz from 12.5 to 16 GHz. The design of this VCO differed from the first one in that it used two varactors in series; possibly the division of rf voltage across the two reduced the low frequency reduction effect we have generally encountered with these hyperabrupt varactors.

The third VCO operated from 15.5 to 18.4 GHz but with an abrupt jump at 16.2 GHz (see Fig. 26(a)) limiting the useful range to 16.5 to 18.4 GHz, which is somewhat less than the normal tuning range shown by the same oscillator with a conventional GaAs varactor (Fig. 26(b)). The tuning curve, however, is definitely more linear; from 16.5 to 17.6 GHz, the tuning curve is a straight line. Further work on this oscillator, including selecting a different T-E diode, might have eliminated the tuning skip and a 15- to 18-GHz range might have been achieved. Since this VCO was constructed with a single varactor from Wafer 1569, the performance of the second oscillator which was much better indicates that the series arrangement of two varactors is a superior approach.

The VCO (5560 V2) shown in Fig. 25(a) was loaned to Westinghouse and to Stanford Research Institute by NESC for evaluation in high-speed set-on systems. It was reported that the tuning speed was extremely fast. After approximately 18 months of usage, the VCO was returned to RCA for repair. The varactor band was rebonded and the unit retested with the results shown in Figs. 27 and 28. Virtually the same tuning range and power were obtained after the long period of usage and the repair. The circuit design of this VCO is described by the drawing of Fig. 29, in which the position and manner of connection to the two plated heat sink GaAs hyperabrupt varactors are shown.

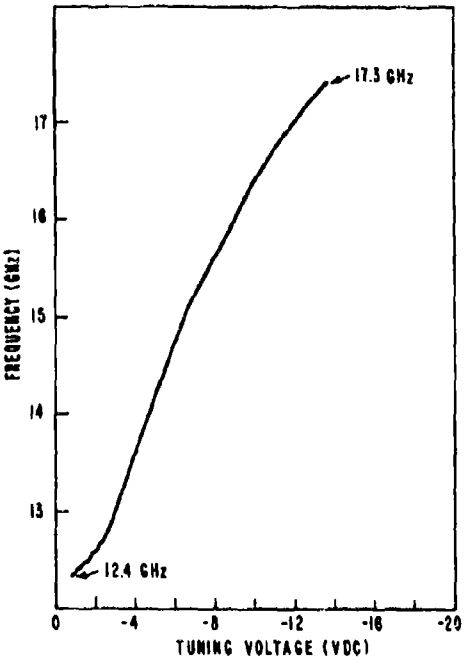

Figure 27. Mid-band VCO tuning curve after repair.

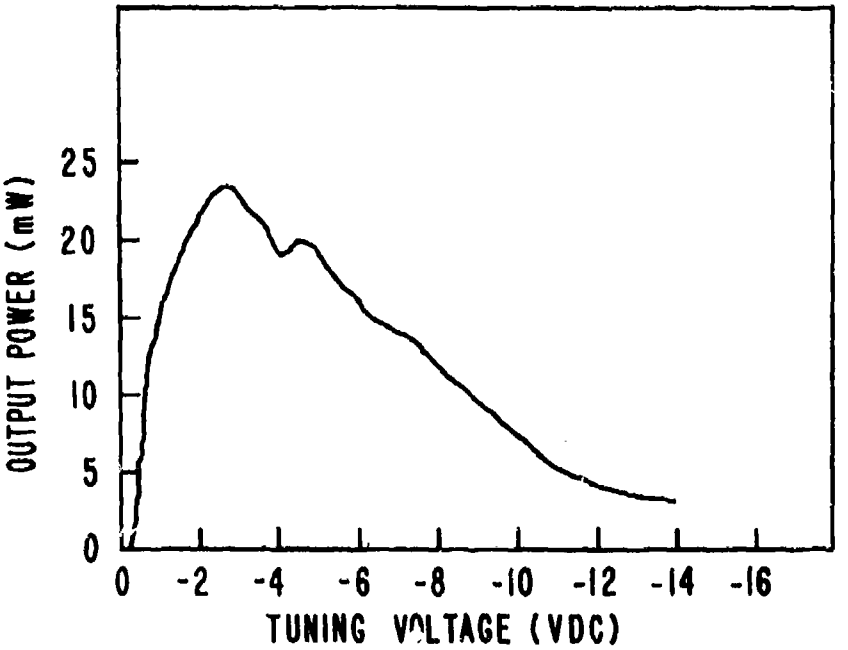

Figure 28. Mid-band VCO power curve after repair.

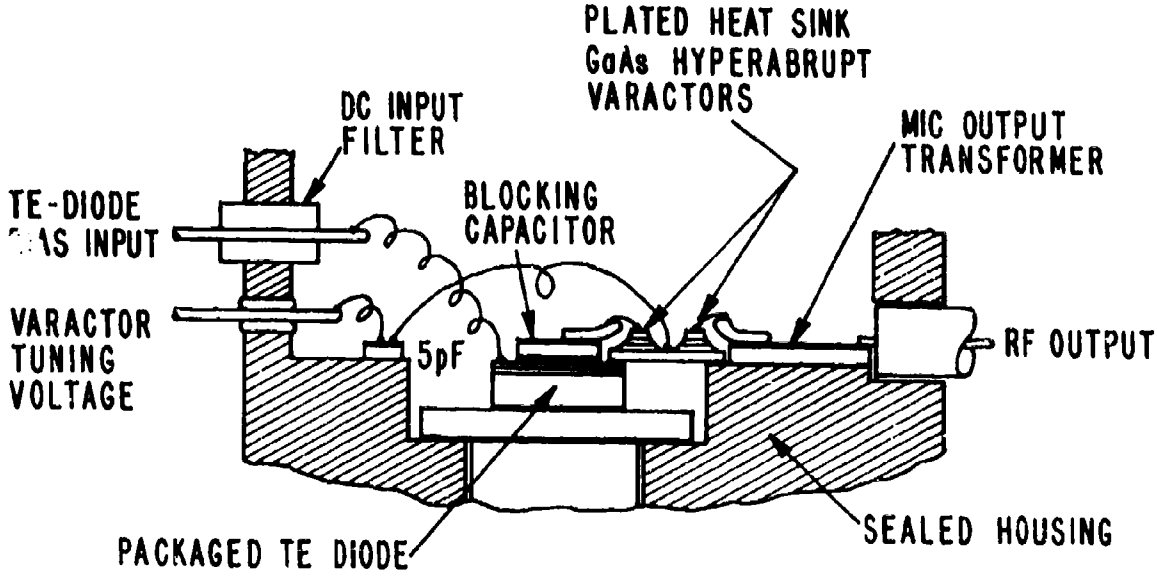

Figure 29. Diagram of mid-band VCO circuit.

At a relatively low frequency and at a low power level using series-connected conventionally mounted varactors from Wafer B408 (with a capacitance ratio of approximately 10:1), more than one octave tuning range was achieved in a fundamental model transistor oscillator as shown by Figs. 30 and 31. In both of these VCOs, the frequency octave band of 2.4 to 4.8 GHz was tuned with about 10% linearity in less than 10 volts.

Both improved linearity and low voltage tuning were obtained in X-band using the conventionally mounted and the plated heat sink varactor diodes in voltage-controlled oscillators, as may be observed in performance curves of Fig. 32 in which almost straight line tuning from 10 to 11 GHz with a swing of only 2.5 V was obtained, and Fig. 33 in which a 3-GHz tuning bandwidth was covered in 12 V with a linearity of approximately $\pm 4\%$. These results are a significant improvement over the tuning curves obtained using conventional abrupt-junction varactors. Despite the large capacitance ratios measured on

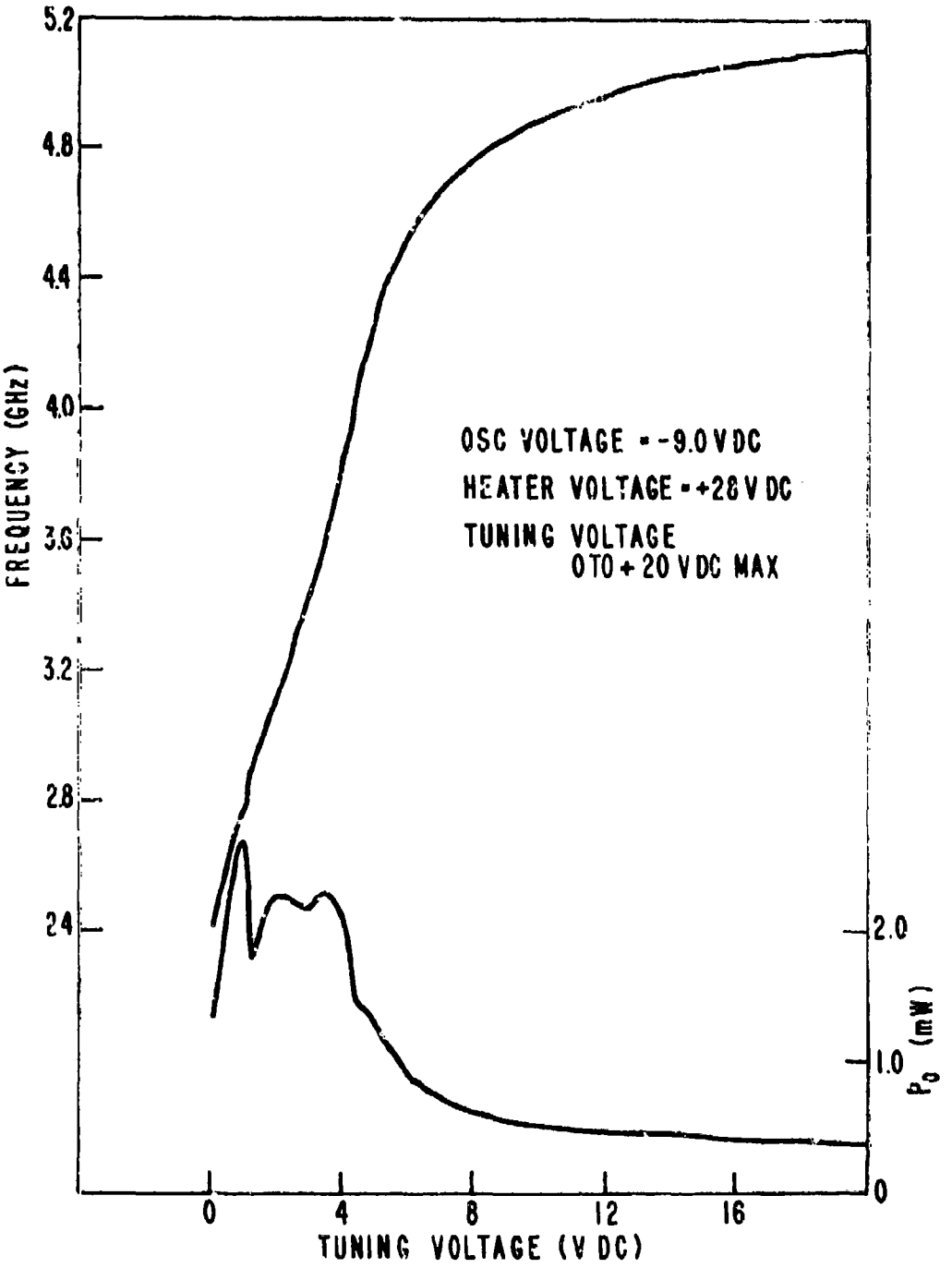

Figure 30. Tuning and power curves of bipolar transistor VCO (No. 1) using GaAs hyperabrupt varactor.

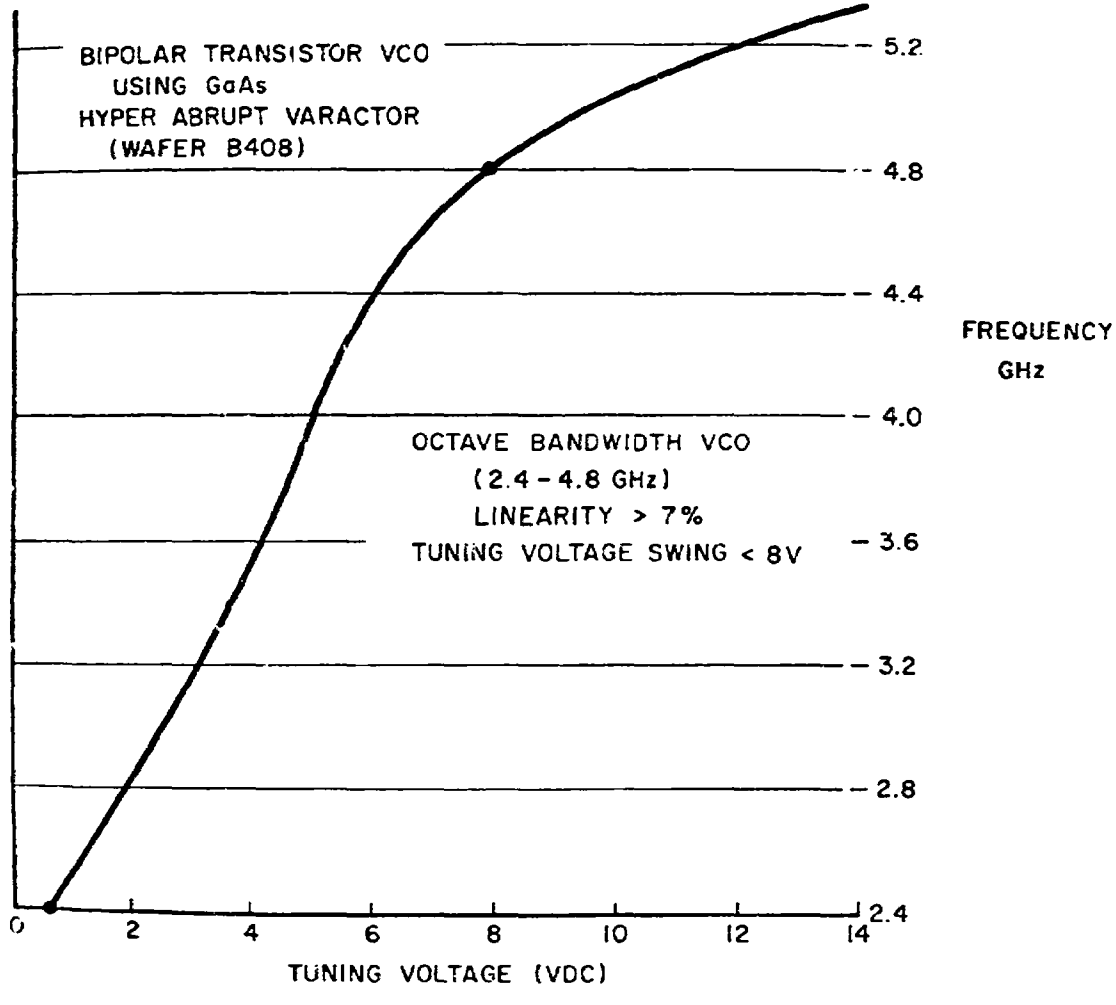

Figure 31. Tuning and power curves of bipolar transistor VCO (No. 2) using GaAs hyperabrupt varactor.

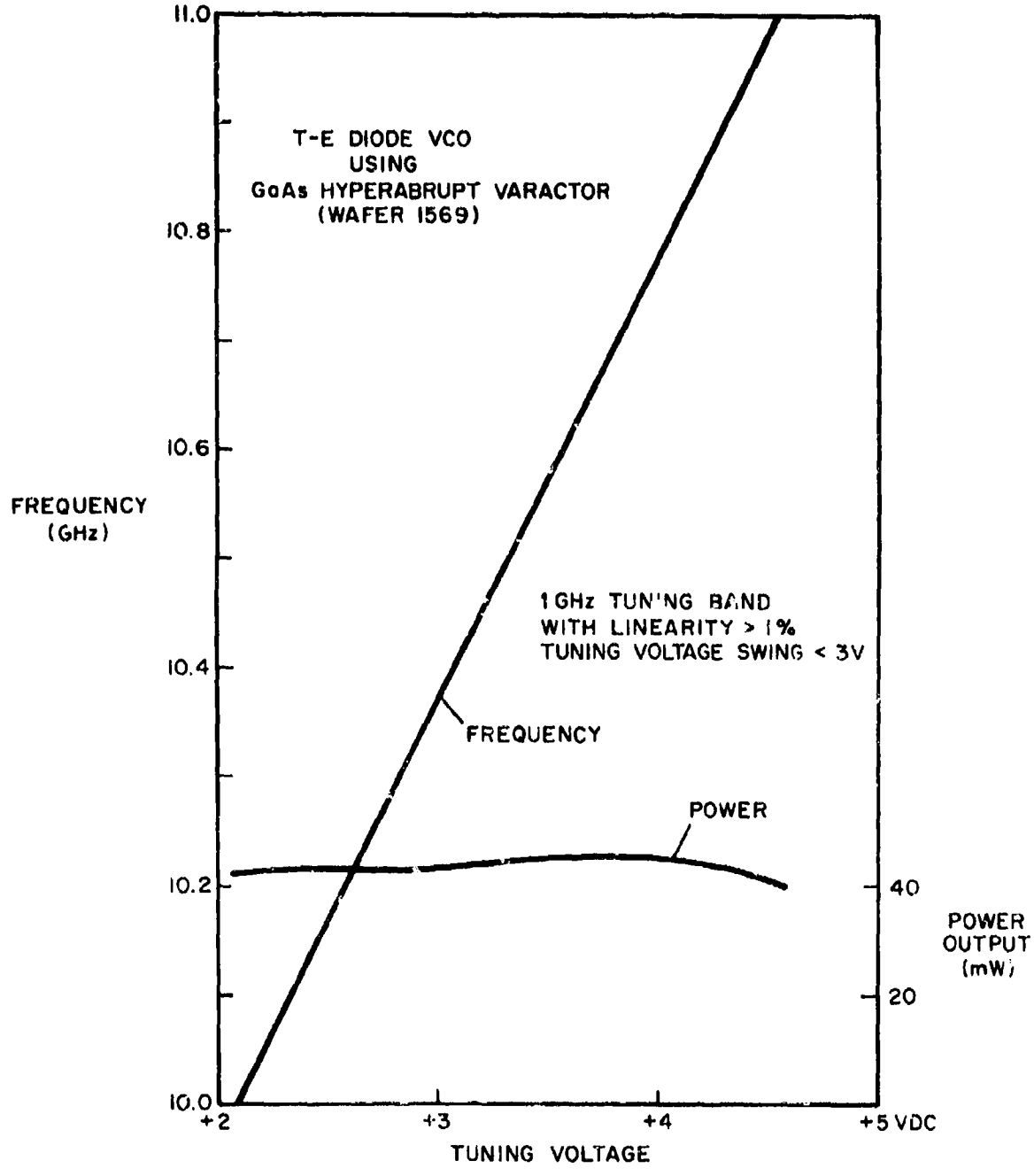

Figure 32. 10- to 11-GHz T-E diode VCO using GaAs hyperabrupt varactor.

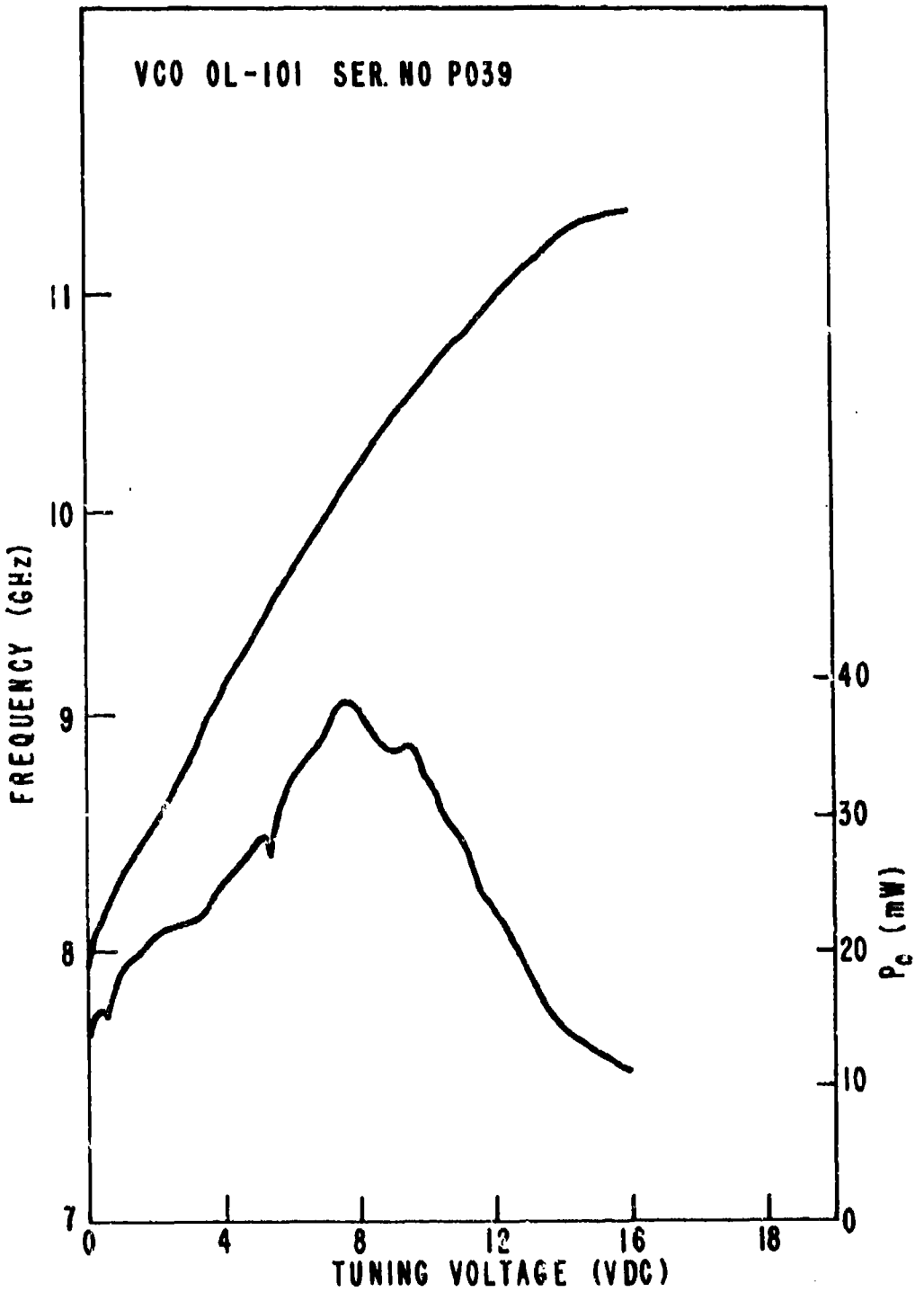

Figure 33. 8- to 11-GHz T-E diode VCO using GaAs hyperabrupt varactor.

these hyperabrupt varactors, however, the voltage-controlled oscillators usually were of lesser total bandwidth than obtained when standard abrupt junction varactors with about 3:1 capacitance ratios were used.

Considerable work was done on this problem, first, by evaluating varactors in a standard X-band VCO, and later by using the earlier-described network analyzer test procedure in which the varactor impedance is measured and plotted at tuning voltages from approximately zero to maximum reverse bias at a different level of applied rf power. An example of one such measurement is shown in Fig. 34. The solid line drawn through the small open circles is the impedance *vs* tuning voltage (from +0.4 to -20 V) as measured with an applied rf power of 12.5 mW at 8 GHz; it covers an arc from -j0.28 to -j1.25 (approximately 80° on the Smith chart). The short dotted line through the small triangles is the impedance variation with the same tuning voltage swing but with 200 mW applied rf power; the change covers a much smaller arc from -j0.95 - j1.4 (approximately 20° on the Smith chart). Neglecting the effect of the capacitance and lead inductance of the package (Type AV 422), the capacitance ratios calculated from these two measurements are 4.5:1 at the 12.5 mW power level but only 1.5:1 with 200 mW incident.

The reduction of tuning capability occurs at the low voltage end of the tuning range which would, as it has proven to be in the operation of the VCOs, limit the lowest frequency which can be obtained. The dashed line through the solid dots of the same Fig. 34 shows the impedance as a function of input power level with the tuning voltage held at zero. From 1.5 mW up to 200 mW, at which level heating effects produce a continuing drift in characteristics, the capacitance value is reduced from approximately 4.0 to 0.45 pF. The probable incident rf power to which the varactor is exposed in a typical transferred-electron diode VCO is 50 mW. At this power level the zero-bias capacitance value would be only about 0.7 pF rather than the 4.0 pF measured with 1.5 mW-incident power. It has been determined that this power level which caused reduction of low-voltage capacitance is present to varying degrees in all of the GaAs hyperabrupt varactors and in the only silicon hyperabrupt varactor which have been measured using this method. Abrupt silicon and abrupt gallium arsenide varactors have not shown the effect as previously indicated in Fig. 21.

A known shortcoming of the use of gallium arsenide varactors in fast set-on VCOs is the tendency to cause a greater post tuning drift than silicon

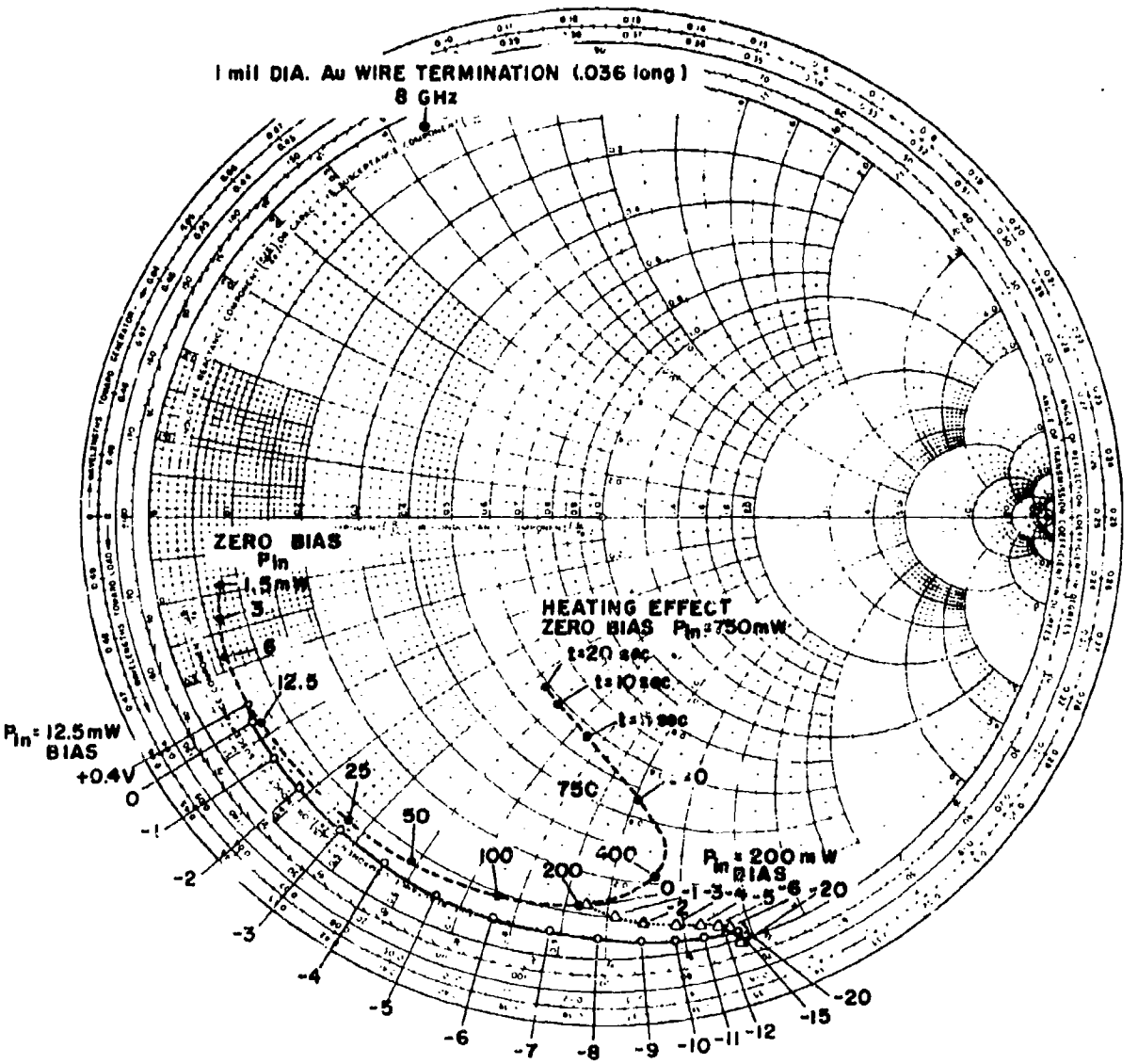

IMPEDANCE OR ADMITTANCE COORDINATES

Figure 34. Smith chart plot of varactor impedance as a function of bias and input power at 8 GHz.

tuning varactors. This can be primarily attributed to the larger thermal resistance of the gallium arsenide substrate compared to silicon. Through the use of the plated heat sink technology described earlier, VCOs fabricated with hyperabrupt varactors so mounted proved to have low post tuning drift rates comparable to standard silicon varactor units.

Measurements of post-tuning drift of an oscillator with a plated heat sink hyperabrupt varactor were made using a special two-level digital memory and D-A converter driver. With this driver and VCO V-105, the following data were taken:

Time (μs)	Frequency Drift After Switching From 10.5 to 8.5 GHz (MHz)	Frequency Drift After Switching From 8.5 to 10.5 GHz (MHz)
1	-5	-13
2.5	-2	~ 5
10	..... Used as reference time for measurement	
25	+1	+ 2
100	+3	+ 2
250	+2	+ 1
1000	+3	0

The 2.0-GHz step from 8.5 to 10.5 GHz required approximately 8 V (250 MHz/V) with the tuning sensitivity varying from 285 to 204 MHz/V at the respective band ends. At the D-A converter 0.025% rated settling time of 2 μs, the driver-caused error should be less than 0.4 MHz. If the D-A-C settling transient follows the normal exponential decay (which it should), the driving voltage should have settled to about 1.5% in 1 second, leaving an approximate error of as much as 31 MHz. Therefore, the validity of the 1-μs readings are of doubtful validity and should not be considered significant.

Longer term drift measurements were made using a counter and recorder from about 1 to 10 seconds. The graphic results are shown in Fig. 35 showing the drift vs time for 3 runs made for both directions of switching between 8 and 10.5 GHz. The drift (and repeatability over a 15 minute period) were in the order of ± 1 MHz.

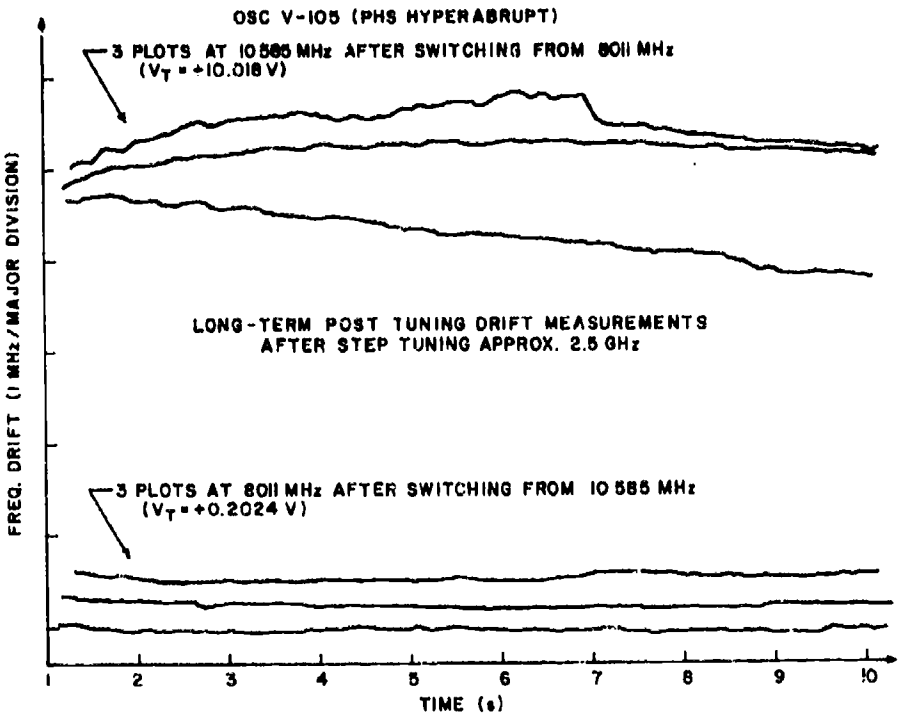

Figure 35. Long-term tuning drift measurements.

As a comparison, in an article concerning VCOs for ECM systems [6], R. N. Buswell of Watkins-Johnson presented test data on an 11- to 14.5-GHz bulk-effect diode VCO in which approximately 20-MHz drift was measured from 10 to 1000 μs, and (very) approximately 2 MHz from 1 to 10 seconds. Based on this singular comparison, the results from the tests on the plated heat sink GaAs hyperabrupt varactor are comparable to or better than results expected with standard silicon abrupt junction varactors.

F. SET-ON VCO FREQUENCY MEMORY SYSTEM

1. Basic Operation

In addition to the deliveries of a number of hyperabrupt gallium arsenide varactors and three voltage-controlled oscillators, the program required the

6. R. N. Buswell, "VCOs in Modern ECM Systems," Microwave Journal, May 1975, pp. 43-46.

deliv ry of a set-on VCO. This work was not completed during the program because of the problems associated with the design of a suitable X-band frequency memory system on which the 11- to 18-GHz set-on VCO was to be based and with the reduced VCO bandwidth effect discussed earlier. Because it is closely related, the work on the X-band frequency memory system will be discussed in some detail.

The Locked-Open-Loop VCO Frequency Memory System which was delivered at the end of the X-band program is shown in Fig. 36. This final version used two basic features: injection locking for reduced set-on time, and discriminator feedback for frequency control. The operation and performance of only the final version will be discussed in this report, although a considerable effort was directed earlier at a somewhat different configuration.

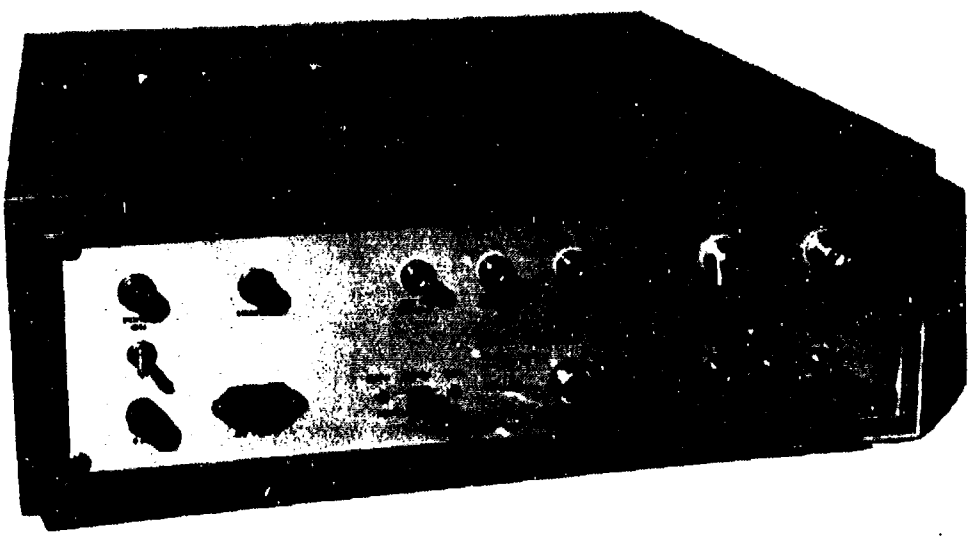

Figure 36. Locked-open-loop VCO frequency memory system.

As may be observed from the block diagram of the modified LOL-VCO-FMS (Fig. 37), the basic components of the open-loop circuit - the limiter, discriminator, follow-and-hold module, linearizer, and VCO - perform the functions of generating and storing an analog voltage related to the frequency of the incoming pulse, and using this to tune a VCO to approximately the same frequency. Since the practical accuracy of an open-loop circuit, which can provide extremely fast approximate set-on, can be shown to be inadequate for the intended application, other components have been added to augment the open-loop circuit and improve the operational accuracy and memory. First, a portion of the input signal is applied through isolators to the VCO to injection-lock it to the incoming signal. This injection-locking process allows the VCO to be set-on *exactly* as soon as the tuning voltage drives the VCO *near* the input frequency, thereby reducing the effective set-on time as well as eliminating any frequency error.

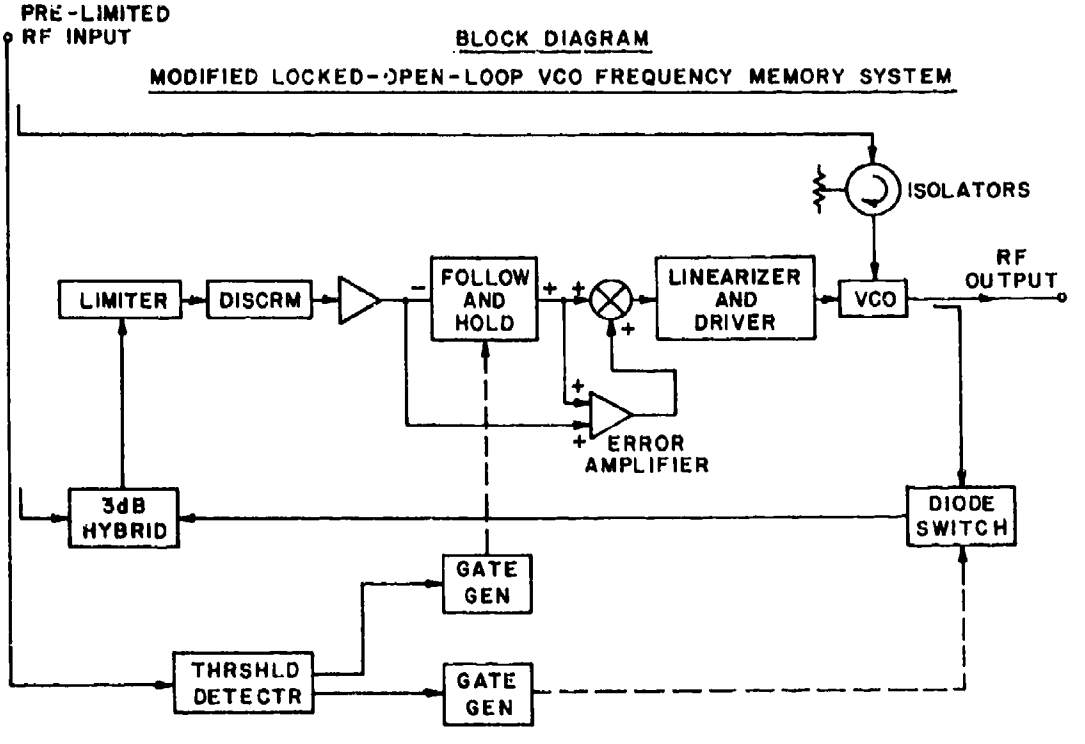

Figure 37. Block diagram of modified locked-open-loop VCO frequency memory system.

In the original configuration of the LOL-VCO-FMS, injection locking was necessary to obtain an accurate feedback reference. In the modified final version, which is being discussed, injection locking is not essential to the operation of the circuit but it does provide an enhancement of initial accuracy, especially for longer duration input pulses.

Vital to the operation of the modified LOL-VCO-FMS is the discriminator feedback control feature. Basically, the output voltage derived from the discriminator during the time the input signal is applied is *remembered* by the follow-and-hold module and used as a reference for comparison with the voltage output of the discriminator after it is switched to monitor the VCO frequency when the reference is established (75 ns). The error voltage generated by the difference between the stored and real-time discriminator outputs is driven toward a null by the gain of the error amplifier in the feedback circuit thereby reducing the frequency error. Timed gate pulses needed to operate the follow-and-hold module and the PIN-diode switch are provided by gate generators which are triggered from a threshold detector. The VCO will remain at or near the input frequency for a time period determined by the duration of the hold command. In the specific form that this VCO frequency memory system is implemented, it is necessary to prevent another input rf pulse from entering the system until this memory runs out, and to limit to some extent the variation of input power level because of the sensitivity of the threshold detector and the effect of gate timing on accuracy.

2. Measurement Method

The key performance criterion of the VCO frequency memory system is the difference between the frequencies of the input pulse and the VCO as a function of time after the pulse. Ideally, the VCO should rapidly set-on to the same frequency and remain at that value for the entire duration of the desired memory time. To measure this time varying frequency difference, a test set-up employing a variable time delay gated spectrum analyzer was used. A block diagram of the test set is shown as Fig. 38. The rf input pulse is produced from a cw signal source by pulsing of a PIN-diode modulator from a variable length pulse generator which also provides a synchronization signal for the other test equipments. Part of the cw output of the signal source is connected

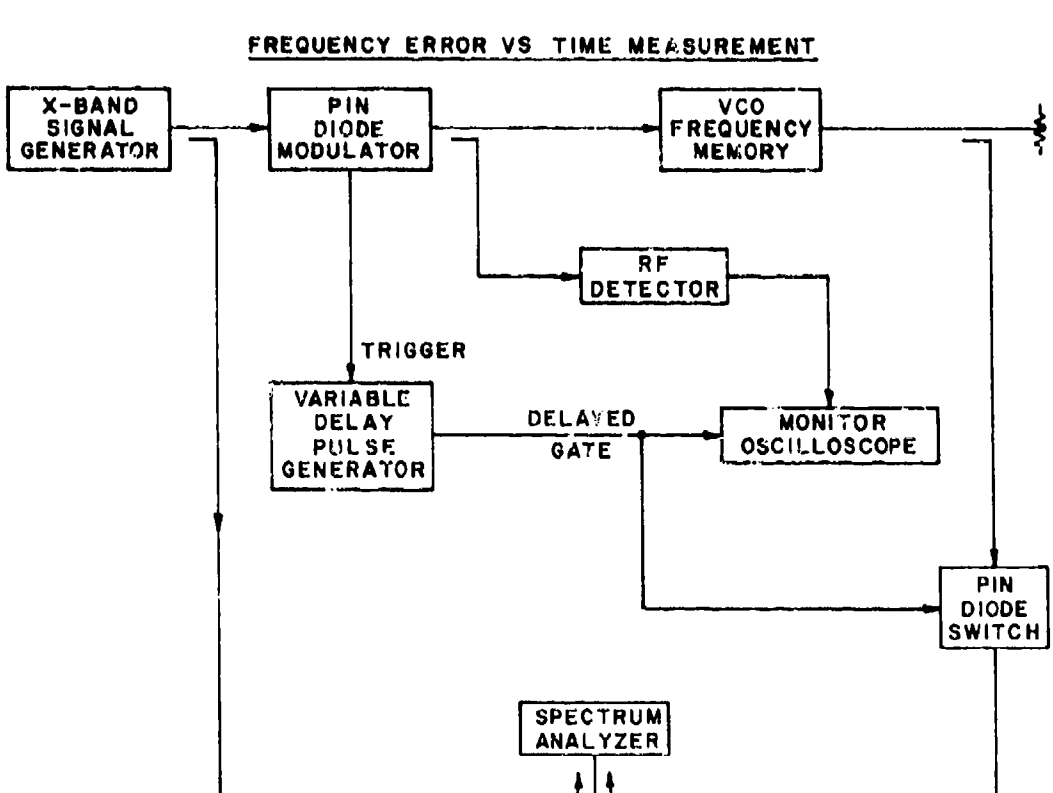

Figure 38. Frequency error vs time measurement.

to the spectrum analyzer through an isolating attenuator and a combining tee. The rf output from the VCO frequency memory system is also connected to the spectrum analyzer through the combining tee after the output signal passes through a SPST PIN-diode switch. This switch is driven from a second pulse generator, triggered from the first, having both variable pulse length and delay provisions. The variable length sets the duration of the sample window; the delay determines the point in time after the input pulse that the output is monitored. With this arrangement, the output frequency in a specified time window, such as $\pm$100 ns centered at 0.1, 1, 10 or 100 µs after the input pulse, may be compared directly with the input reference frequency since both are simultaneously displayed on the spectrum analyzer. The difference between the cw input line spectrum and the nominal center of the sinx/x spectrum generated

by the PIN-diode switch chopping of the VCO output signal can be readily measured using the calibrated dispersion of the spectrum analyzer as may be seen from the example shown in Fig. 39. Data are taken at various input frequencies at different delay settings to provide a series of frequency error vs time graphs.

3. Test Data

The frequency error vs time measurements performed on the delivered VCO frequency memory system are presented in a series of graphs in Figs. 40 through 50. In the first group, Figs. 40 through 47, the system was tested with an input pulse length of 250 ns and data were taken at 9.2, 8.5, 9.0, 9.5, 10.0, 10.2, 10.5 and 11.0 GHz. Reasonably good performance with errors of less than 5 MHz was obtained over the 8.2- to 10.2-GHz bandwidth from about 0.7 to beyond 80 μs. As is evident in the first six of the graphs, the error in the 100- to 200-ns interval is approximately zero because of the injection locking. Actually, the VCO frequency is precisely the same as that of the input pulse from about 75 to 250 ns, but the averaging effect of the ±100 ns measurement gate obscures the accuracy.

As the input pulse ends, the discriminator feedback circuit takes over and begins to correct the open loop error. The correction time and residual error vary with input frequency because of variations in the open loop accuracy across the band and for other causes which will be discussed later. The long-term memory is excellent; from approximately 1 to 80 μs there is virtually no memory decay and the errors stay within 3 MHz. At some test points, measurements have been made to 1 ms with about the same low error. This excellent memory is obtained because of the bootstrap effect the feedback circuit has on the follow-and-hold module which will be described in a subsequent section on the components of the system.

To demonstrate that the system accuracy is enhanced by, but not dependent upon the use of the injection locking, several error vs time measurements were performed with 75-ns duration input pulse. Graphs of the results are shown in Figs. 48 through 50(a). Without the effect of the injection locking, the initial error is considerably greater, but as again obscured by the measurement averaging, follows the same general correction time response and ends up with the same accuracy and excellent memory. In fact, the correction time is

(a)

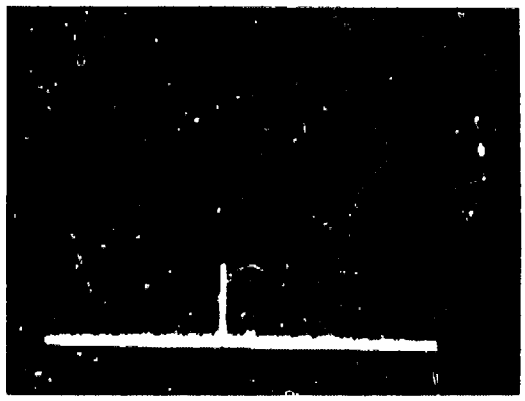

SPECTRUM ANALYZER
DISPERSION
10 MHz/CM

CENTER FREQUENCY
9.0 GHz

OSCILLOSCOPE PHOTO SHOWING TIME RELATION BETWEEN RF INPUT AND MEASUREMENT GATE.

(b)

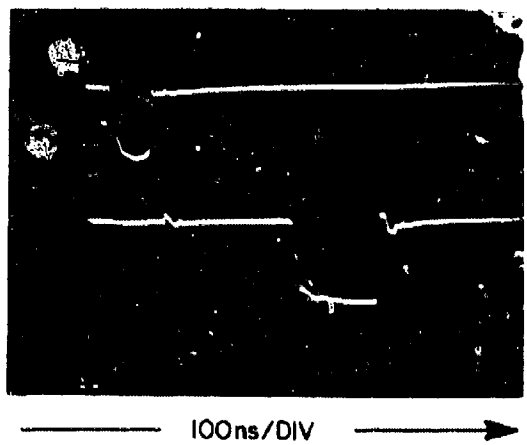

DETECTED RF INPUT PULSE (5mV/DIV)

VARIABLE DELAY PULSE TO PIN-DIODE SWITCH FOR MEASUREMENT GATE (1V/DIV)

100ns/DIV

Figure 39. (a) Spectrum analyzer photo of cw reference and gated output of unit under test showing frequency error at time of measurement gate. (b) Oscilloscope photo showing time relation between rf input and measurement gate.

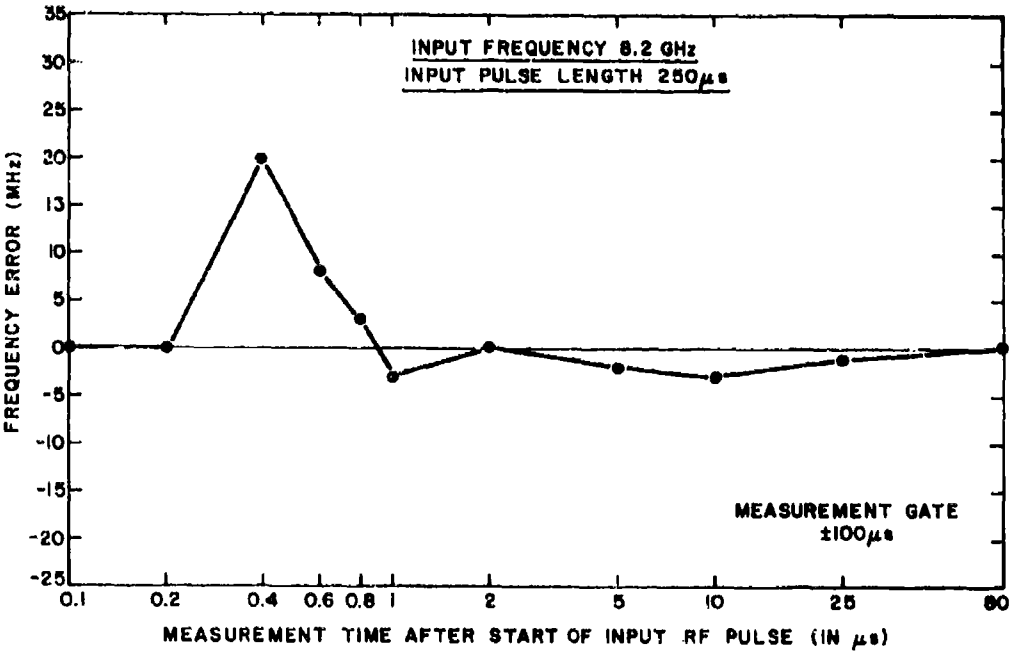

Figure 40. Input frequency 8.2 GHz, input pulse length 250 ns.

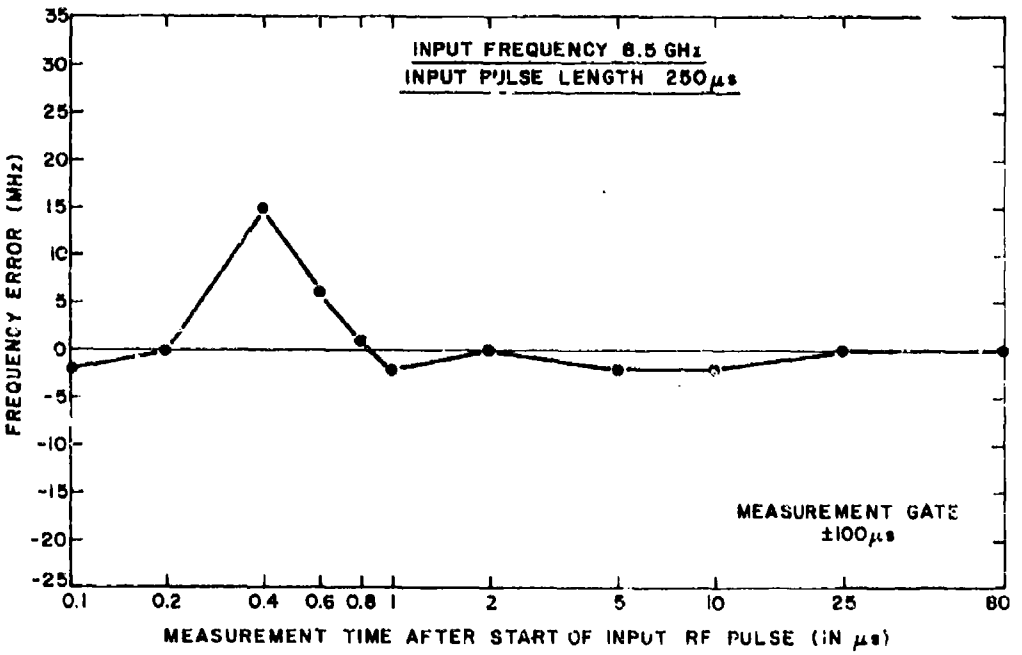

Figure 41. Input frequency 8.5 GHz, input pulse length 250 ns.

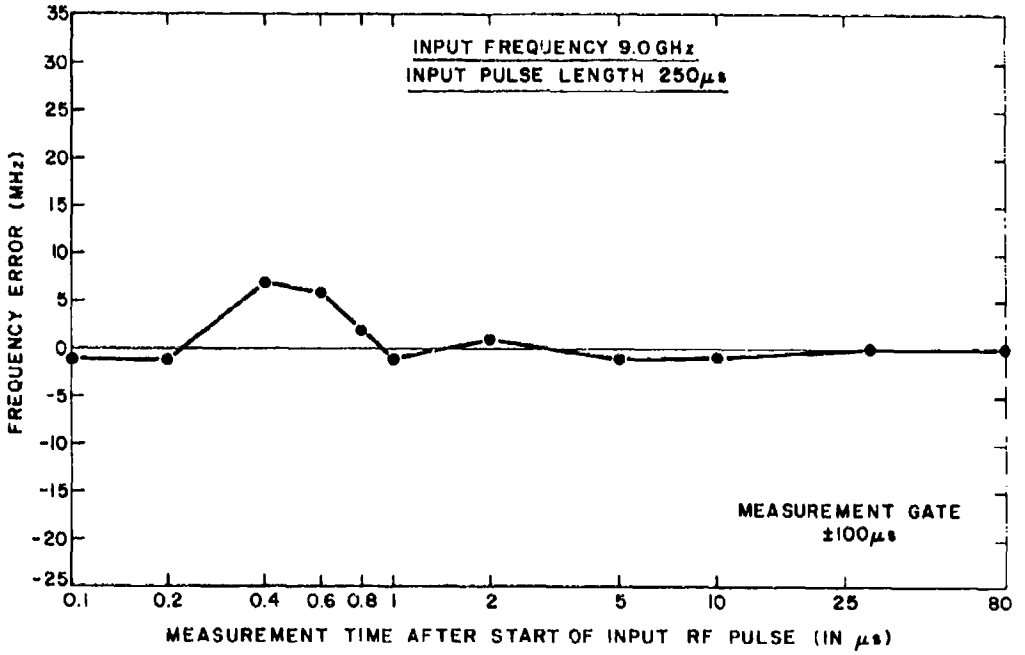

Figure 42. Input frequency 9.0 GHz, input pulse length 250 ns.

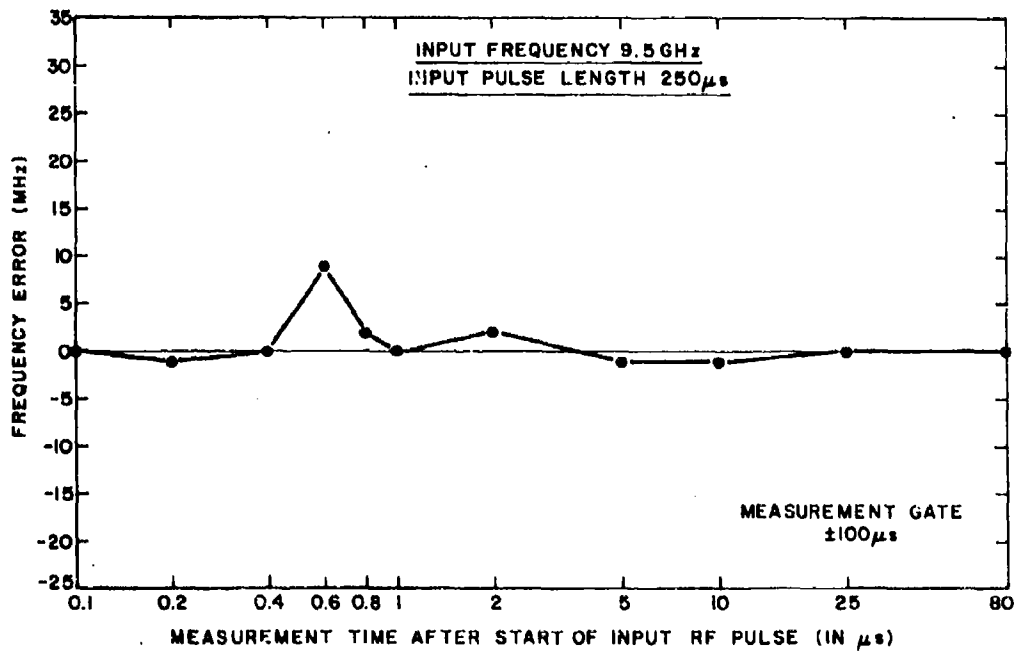

Figure 43. Input frequency 9.5 GHz, input pulse length 250 ns.

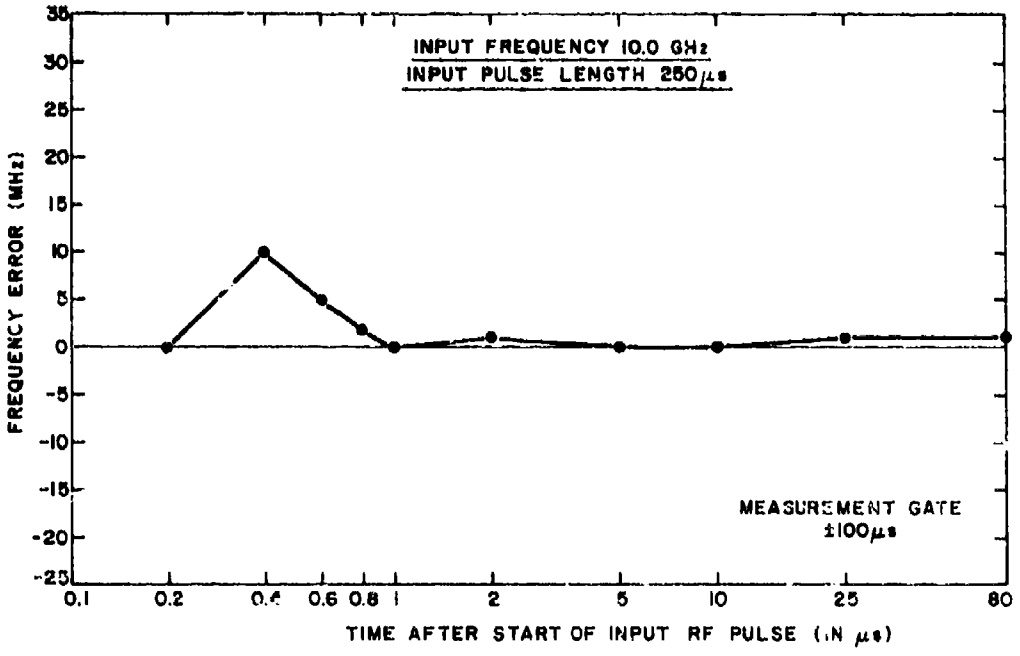

Figure 44. Input frequency 10.0 GHz, input pulse length 250 ns.

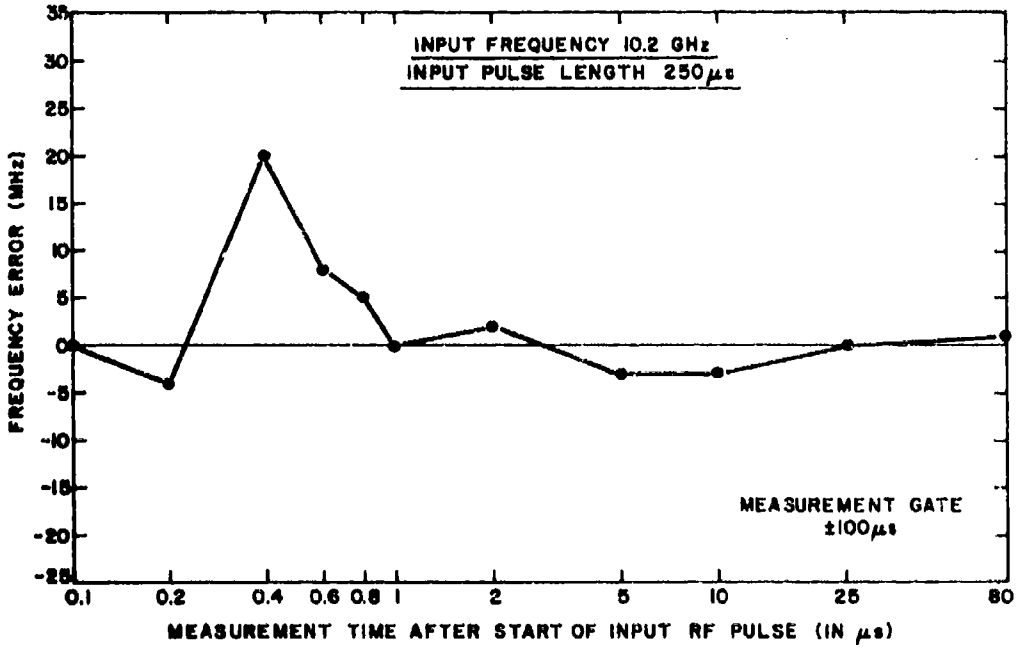

Figure 45. Input frequency 10.2 GHz, input pulse length 250 ns.

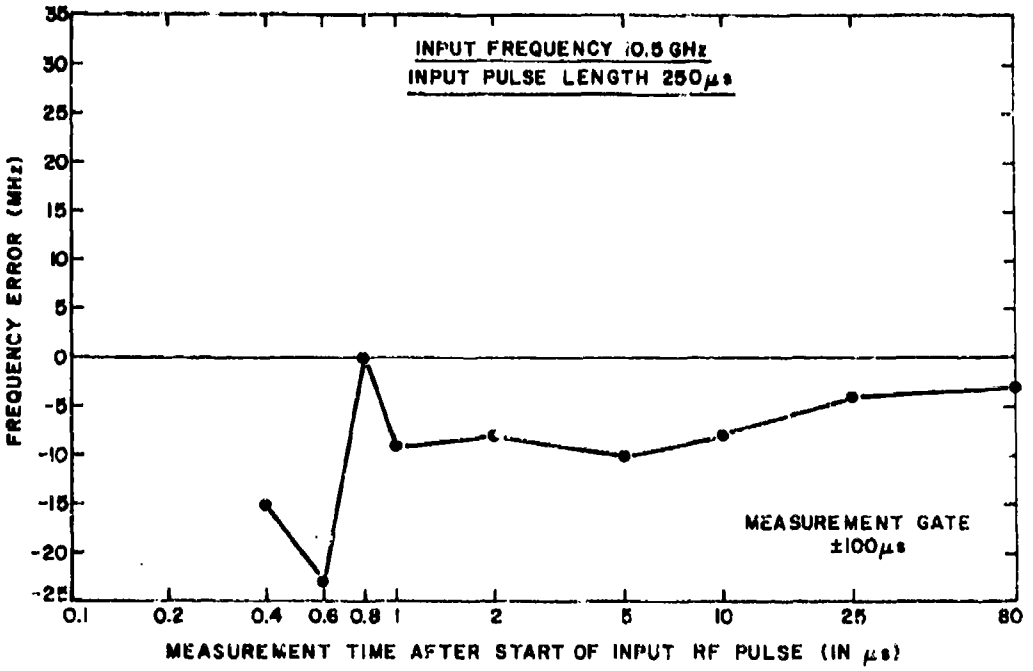

Figure 46. Input frequency 10.5 GHz, input pulse length 250 ns.

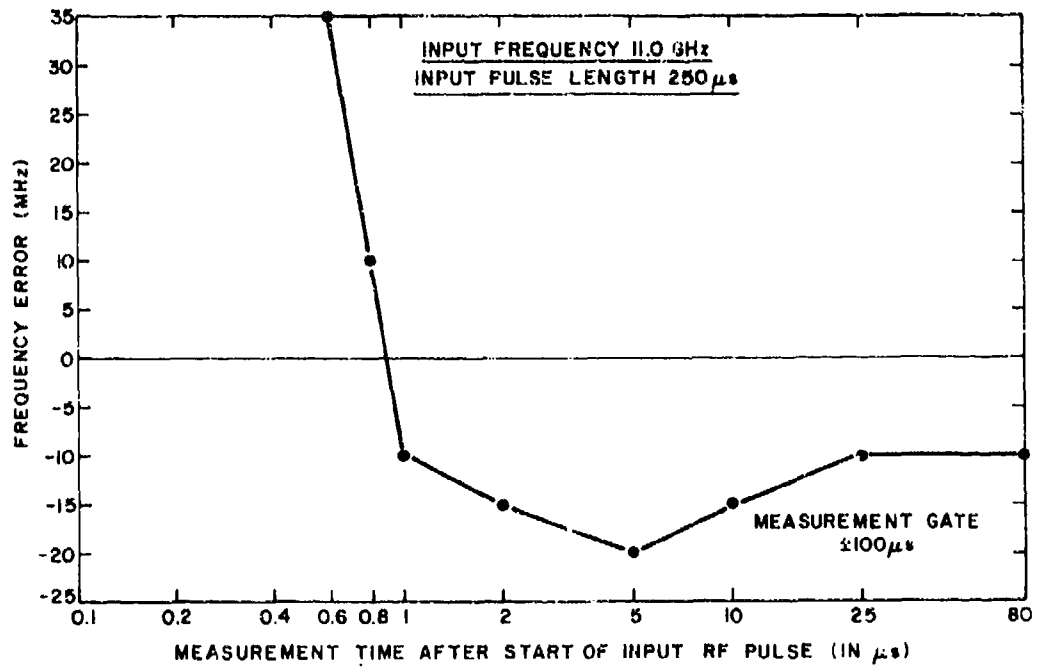

Figure 47. Input frequency 11.0 GHz, input pulse length 250 ns.

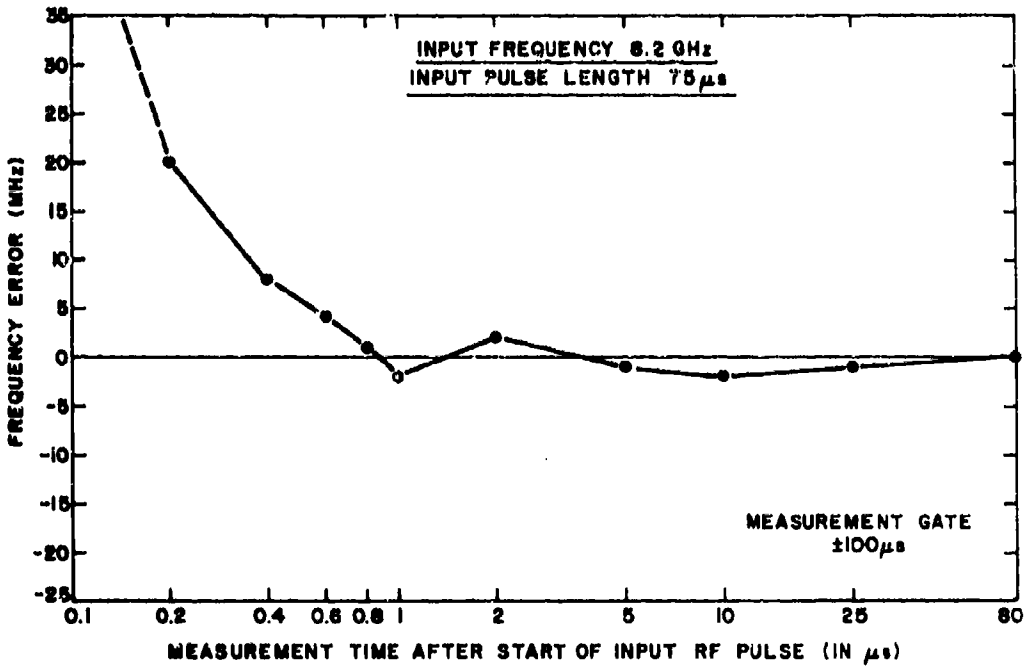

Figure 48. Input frequency 8.2 GHz, input pulse length 75 ns.

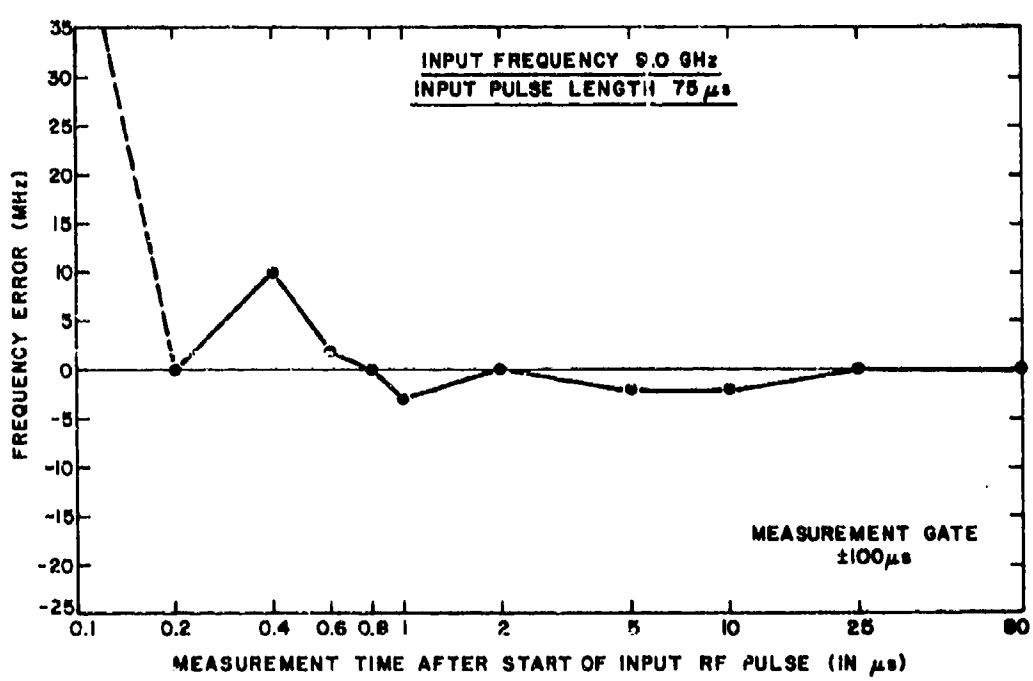

Figure 49. Input frequency 9.0 GHz, input pulse length 75 ns.

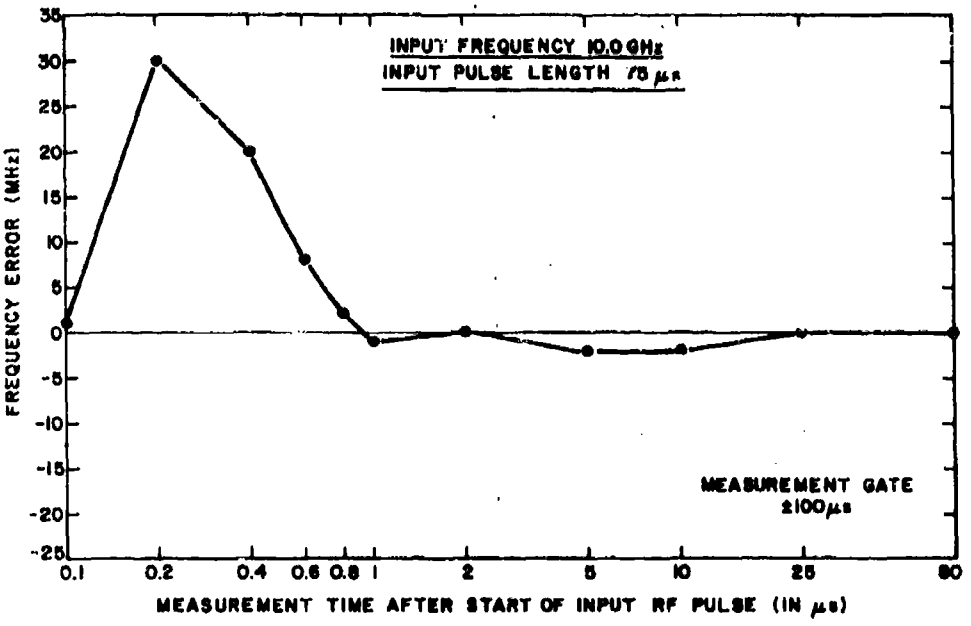

(a)

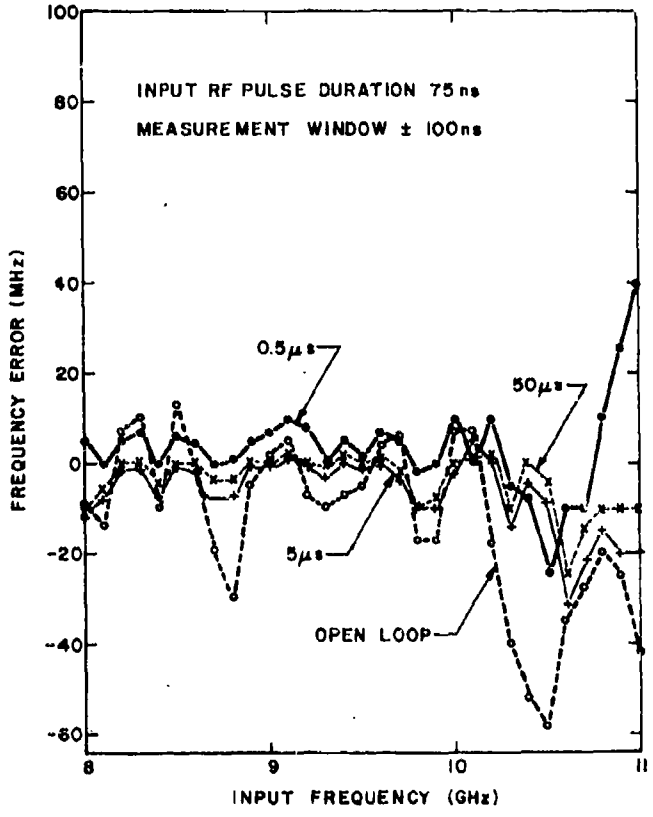

(b)

Figure 50. (a) Input frequency 10.0 GHz, input pulse length 75 ns. (b) Frequency error vs input frequency.

slightly better because the error voltage is developed sooner from the discriminator - by the difference of the two different measurement pulse durations (250 - 75 ns).

This series of measurements shows that the LOL-VCO-FMS can function with input pulse lengths as short as 75 ns with no significant loss in short- or long-term accuracy. For longer pulses, in the microsecond range, the injection locking mechanism will cause the output to track exactly from about 75 ns until the input pulse ends, at which time the correction response starts and the memory is established with the same approximate accuracy. The system, as arranged, does not require input pulse length normalizing.

Figure 50(b) presents the frequency error vs time performance in a different manner. The error is plotted as a function of bandwidth from 8.0 to 11.0 GHz for 0.5-, 5.0-, and 50-μs measurement points referenced to the start of the input pulse. Data points are shown at 100-MHz intervals across the band for these memory times and are consistent with the previous graphs which were made for only eight different frequencies.

By disabling the feedback circuit internally it was possible to measure and plot the open loop performance on this same graph for information only. At no time does the circuit operate normally in this mode. The open loop results show the magnitude of the residual error which is reduced substantially by the discriminator feedback circuit.

Summarizing the measured data, the LOL-VCO-FMS provides an output frequency which is generally within 5 MHz of the input pulse frequency from 8.2 to 10.2 GHz over the time span from about 600 ns to well beyond 80 μs when driven with a 75-ns pulse. With longer input pulses, exact frequency set-on is achieved in about 100 ns until the pulse ends, at which time accurate frequency storage is obtained after the feedback recovery transient is completed.

SECTION III

CONCLUSIONS

A method for fabricating and processing plated heat sink hyperabrupt gallium arsenide varactors for use in microwave voltage-controlled oscillators was developed and evaluated during this program. VCOs fabricated with these varactors demonstrated considerably improved linearity and reduced tuning voltage requirements as compared with VCOs fabricated with conventional abrupt junction varactors.

During the program, hyperabrupt gallium arsenide varactor wafers were grown in which values of γ from 0.5 to 2.0 were obtained and capacitance ratios as high as 30:1 were measured. In most cases, the carrier concentration profiles necessary to obtain the various hyperabrupt characteristics obtained were grown epitaxially by the hydride vapor synthesis technique using a programmed controller to introduce dopant at the required rates. The process was proven to have the capability to grow wafers which closely matched a desired profile. Because of the versatility of this controlled back-doping process, complicated structures can be grown such as the p^+-n_o-n^+-n-p^+ GaAs wafers which were used to produce electrolytically etched varactor diodes with integral heat sinks. These plated heat sink mounted varactors proved to have very low post tuning drift characteristics in VCOs compared with conventionally mounted GaAs varactors.

Voltage-controlled oscillators fabricated with the hyperabrupt GaAs varactors proved to have considerably better linearity and required lower tuning voltage swings than VCOs built using conventional step-abrupt junction varactors. Nearly straight line tuning characteristics were obtained over as much as 2 GHz in S-band, 2.5 GHz in X-band, and 4.5 GHz in Ku-band. Tuning voltage swings for these bandwidths were in the order of only 10 V rather than the 40 V which VCOs with conventional varactors would require. Less than expected overall bandwidth was obtained from these VCOs because of a significant reduction in the maximum junction capacitance of the hyperabrupt varactor in the presence of applied rf signal.

The basic design of a set-on VCO frequency memory was completed and demonstrated on a related program in X-band but was not implemented in Ku-band,

as had been originally intended. In this related program, a VCO frequency memory system was designed, fabricated, and demonstrated which uses a combination of rapid open-loop set on, injection locking, and discriminator feedback control to respond to unknown frequency incoming pulses as short as 75 ns by setting a VCO to within 5 MHz of that frequency in less than 600 ns and holding it within the same accuracy for periods of time well beyond 80 μs. Longer duration input pulses produce exact set-on during the pulse through injection locking, but immediately following the input signal, there is a transient offset of approximately 400 ns while the feedback circuit stabilizes, after which the frequency error is reduced and held under 4 MHz for nearly 1 ms. Results obtained late in the hyperabrupt varactor VCO program have shown that comparable or better set-on VCO results should be obtainable using a single VCO covering 11 to 18 GHz.

SECTION IV

RECOMMENDATIONS

The results obtained during this program have demonstrated significant improvements in linearity and reduced tuning voltage which can be obtained in VCOs for ECM type applications with hyperabrupt GaAs varactors. In Ku-band, continuous tuning of a single VCO covering almost 11 to 18 GHz was demonstrated. It is recommended that additional effort be directed toward the fabrication of an 11- to 18-GHz Single VCO Frequency Memory System based on the design demonstrated during the X-band Locked-Open-Loop VCO Frequency Memory System Program.

With some additional improvements in the hyperabrupt varactors, the VCO design, and the memory system concepts, it is expected that comparable frequency set-on and memory performance can be obtained over the 11- to 18-GHz band as was demonstrated from approximately 8 to 10.5 GHz in the X-band system. It is also recommended that some additional effort be applied to determining the specific causes of the reduction in low voltage capacitance with applied rf signal which substantially reduces the potential VCO bandwidth.

REFERENCES

1. S. M. Sze, *Physics of Semiconductor Devices*, (Wiley-Interscience, New York, 1969), pp. 114-116.

2. J. J. Tietjen, R. E. Enstrom, V. S. Ban and D. Richman, "Vapor-Phase Growth of Several III-V Semiconductors," Solid State Technology, pp. 42-49, (October 1972).

3. C. J. Nuese and J. J. Gannon, "Electrolytic Removal of P-Type GaAs Substrates from Thin, N-Type Semiconductor Layers," J. Electrochem. Soc. 117, 8, 1094-1097 (1970).

4. E. J. Thrusti, "A Method for Selective Substrate Removal from Thin P-Type Gallium Arsenide Layers," J. Phys. E, 7, 493-495 (1974).

5. J. Collard, et al., *Microwave Semiconductor Diode Research*, Final Report, ECOM-0581-F, March 1969.

6. R. N. Buswell, "VCOs in Modern ECM Systems," Microwave Journal, May 1975, pp. 43-46.